Noise Investigations for the Tracker Turicensis of the LHCb Experiment

---

Master Thesis

Mathematisch-naturwissenschaftliche Fakultät
der

Universität Zürich

Viktor Hangartner

Prof. Dr. Ulrich Straumann
Dr. Olaf Steinkamp
Dr. Jeroen van Tilburg
Dr. Mark Tobin

Zürich
August 2009

Abstract

The LHCb Tracker Turicensis is a silicon micro strip detector with low signal-to-noise ratio. On strip recorded data is buffered in a pipeline, numbered for synchronisation purposes and serialised for transmission within the data acquisition system. These processes affect both pedestals and noise. In this thesis, a method to calculate the noise taking into account the pipeline column number and its encoding is described. Furthermore, the effect on pedestals related to the pipeline column number and monitoring of low noise channels will be described.

Contents

Chapter 1

Introduction

The Large Hadron Collider (LHC) [1] at CERN will provide proton-proton collisions at centre-of-mass energies of up to 14 TeV at a rate of about 30 MHz. As a result of these collisions, about 10^{12} $b\bar{b}$ quark pairs per year will be produced at a luminosity of $2 \times 10^{32} \mathrm{cm}^{-1}\mathrm{s}^{-1}$ and hadronise into B mesons or baryons.

Within the Standard Model, CP-violation can be generated by a single phase in the complex Cabbibo-Kobayashi-Maskawa matrix (CKM matrix) describing the quark couplings in charged current interactions. The level of CP violation required to explain the asymmetry of matter and antimatter observed in our Universe is several orders of magnitude above the Standard Model's expectation. Therefore, one searches for additional sources of CP violation.

To study CP violation in detail one investigates the decay modes of B mesons. The standard tree-level decay is suppressed for some B mesons. This allows experimental measurements of rare higher-order decay modes. Due to the high b quark production cross section in the LHC, enough statistics will be provided to allow precise measurements of such rare processes. These measurements might unveil deviations from the Standard Model and lead to the detection of new sources of CP violation. The LHCb experiment is designed to perform such measurements in a wide range of B meson decays with the highest precision possible.

1.1 The LHCb Experiment

The LHCb experiment is designed as a single-armed forward spectrometer. Since $b\bar{b}$ pairs at the LHC are produced with a considerable boost, both B mesons and their decay products are contained within a cone around the beam direction. B mesons are produced instantaneously in the proton-proton collision at at the primary vertex. The secondary vertex marks the decay of the B meson and is displaced about 10 mm with respect to the

primary vertex. The acceptance of the experiment is designed to cover the forward cone as much as possible leading to the overall dimensions of the experiment of roughly 6m x 5m x 20m. The LHCb experiment is located about 100 m under ground.

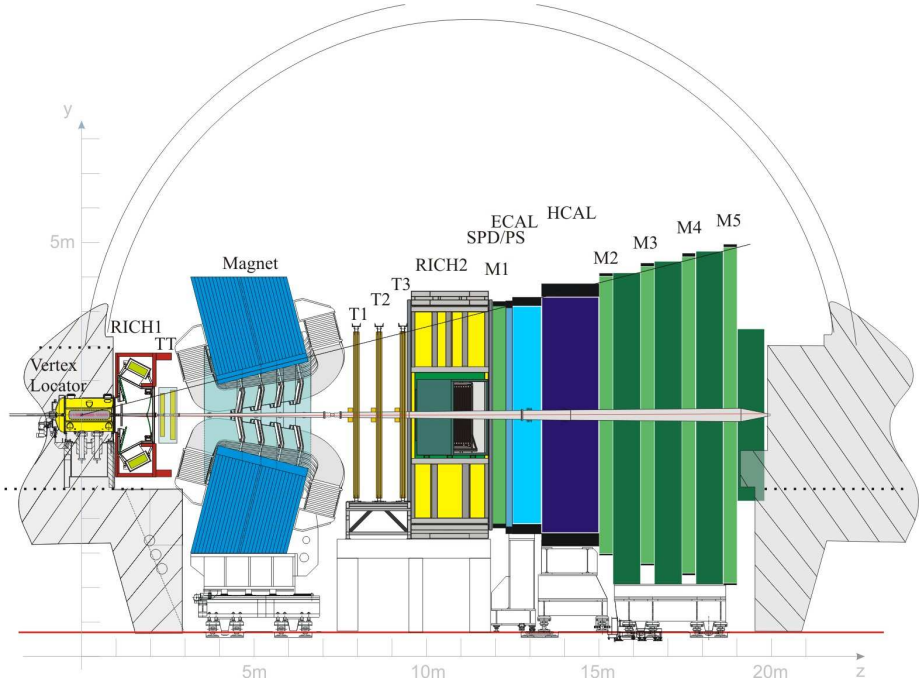

Figure 1.1: A side view of the LHCb experiment to the vertical plane. The LHCb sub-detectors are: Vertex Locator (VELO), Tracker Turicensis (TT), Inner and Outer Trackers (T1 – T3), ring imaging Cherenkov detector 1 (RICH 1), RICH 2, electromagnetic and hadronic calorimeters (ECAL, HCAL), muon stations (M1–M5), scintillating particle detector (SPD) and the pre-shower detector (PS).

The LHCb experiment consists of several sub-detectors and a dipole magnet to bend charged particles to allow precise momentum determination, see Figure 1.1. There are two categories of sub-detectors, the tracking detectors and the particle identification detectors.

Tracking detectors: Vertex Locator (VELO), Tracker Turicensis (TT), Inner and Outer Tracker (IT, OT).

Particle identification detectors: Ring imaging Cherenkov detector 1 (RICH 1), RICH 2, electromagnetic and hadronic calorimeters (ECAL, HCAL), muon stations (M1–M5), Scintillating Particle Detector (SPD) and the Preshower Detector (PS).

The tracking system of LHCb consists of four sub-detectors and permits to reconstruct trajectories and momenta of charged particles. It is built closely around the proton-proton interaction point and is designed to measure trajectories of charged particles very accurately. This is important as primary and secondary vertices are separated by only a few millimetres and need to be reconstructed precisely. The main tracking system consists of four tracking stations located before and after the magnet. The TT is located before and the three tracking stations T1 – T3 consisting each of an IT and OT station are located after.

Except for the OT which is a straw tube detector, all sub-detectors involved in the tracking are based on silicon micro-strip technology and therefore use to a certain extent the same hardware parts. In particular, the TT and the IT use the same front-end chip and data acquisition chain and are part of the same detector group called the Silicon Tracker.

1.2 Tracker Turicensis

The TT detector contains about 900 silicon micro strip sensors distributed over four detection layers, with an approximate size of $1.8\,\mathrm{m}^2$ per layer. TT sensors are produced by HPK Hammamatsu, Japan. The sensors are 500μm thick, 9.64 cm wide and 9.44 cm long. They have 512 readout strips and the strip pitch is 183 μm. All sensors inside the TT detector must be precisely placed to allow track reconstruction within $\pm 50\,\mu$m. In addition, they all have to be connected to readout electronics, high and low voltage supplies. Therefore sensors are grouped into half-modules (Figure 1.2) containing 7 sensors in a row. A total of about 30 half-modules per layer cover the acceptance of the experiment as indicated in Figure 1.3. On a module, sensors are grouped into two or three readout sectors. Within a readout sector, the 512 silicon strips of the different sensors are connected strip by strip through wire bonds. As particle flux increases close to the beam pipe, small readout sectors, i.e. short readout strips, are required in the central part of the detector to achieve appropriate hit occupancies. Therefore the six sensors around the beam pipe are read out separately (yellow marked sensors in Figure 1.3) and two different types of modules are in use:

- 4-3 modules: the sensors are split into two readout sectors. A long one called L containing four sensors and a shorter one called M3 containing 3 sensors.

- 4-2-1 modules: the sensors are split into three readout sectors. The L sector (4 sensors), M2 sector (2 sensors) and the short K sector containing the single sensor near the beam pipe.

The total strip length is between 38 cm for the L sector and 9 cm for the single K readout sector close to the beam-pipe, see Table 2.4.

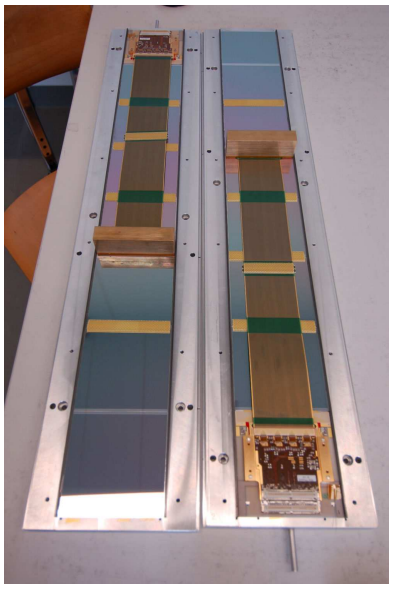

Figure 1.2: Photograph of the front-side of two modules in their production templates. Readout hybrids are located at one end of each module. The M section is connected through a Kapton cable to its front-end readout hybrid carrying 4 Beetles.

At one end of the modules front-end readout hybrids are located. Each hybrid contains four radiation hard readout chips called Beetles [3] and provides connection to backend readout electronics and mechanical connection to the support frames. There is a hybrid for each readout sector of the module.

A Beetle can read out 128 channels and is connected with the same number of readout strips via a short pitch adapter for the L section and via Kapton cable in case of M and K sectors. The pitch adaptor is needed as the 128 bond-pads on the Beetle side are staggered in four rows, whereas on the Kapton cable or the sensor the 128 channels are beside each other. The connection from the Beetle to the pitch adaptor is provided by bond wires. Figure 1.5 shows the four layers of bonds from the Beetle (bottom) to the pitch adaptor (top). The signals read out leave the Beetle via four analogue output lines referred to as ports.

Overall, there are 892 silicon sensors on 128 modules, of which 24 are 4-2-1 type modules. The numbers of readout sectors, Beetles ports and strips are given in Table 1.1.

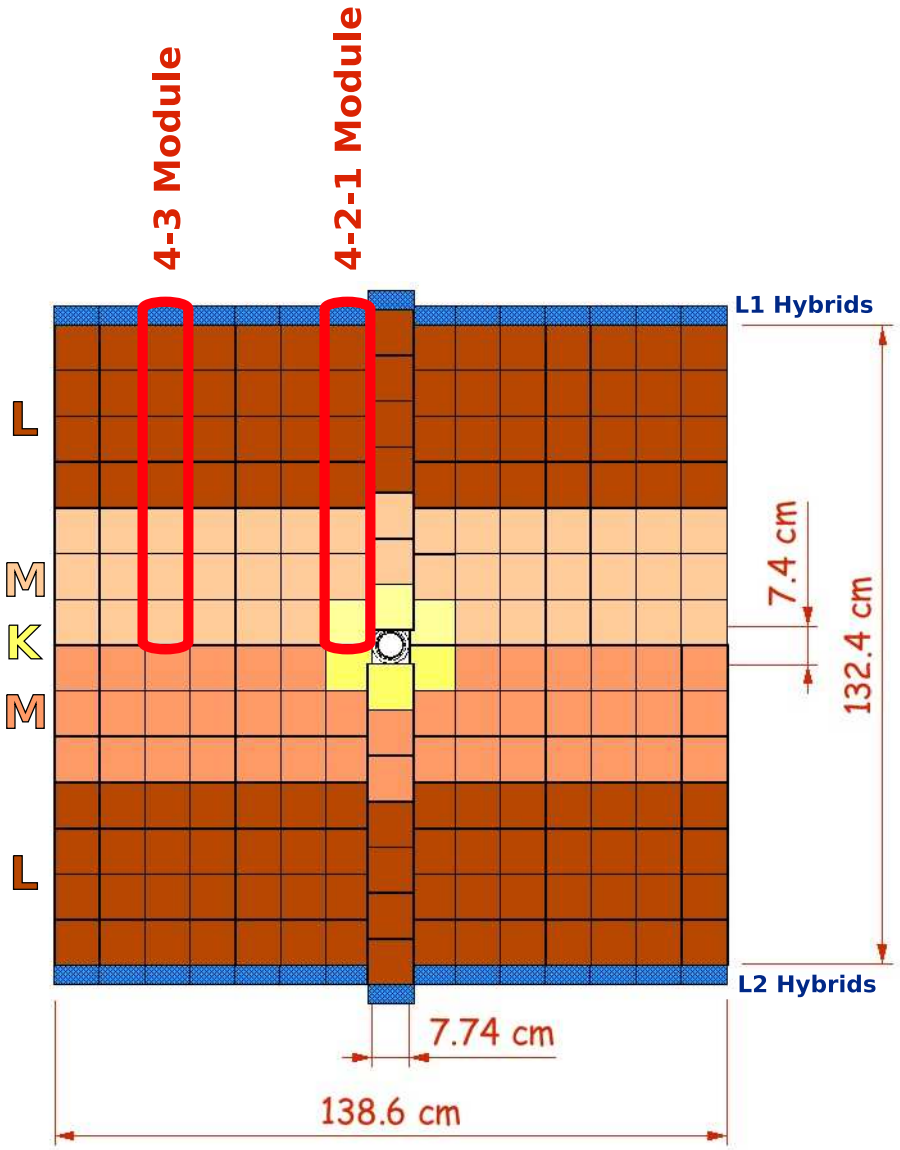

Figure 1.3: Sketch of one of the four silicon planes of the TT station (TTa x-layer) consisting of 14 full-modules, i.e two half-modules glued together end-to-end, and two "4-2-1 type" modules covering the middle part above and below the beam pipe. Each rectangle symbolises a silicon micro strip sensor. Readout sectors are marked in different colours.

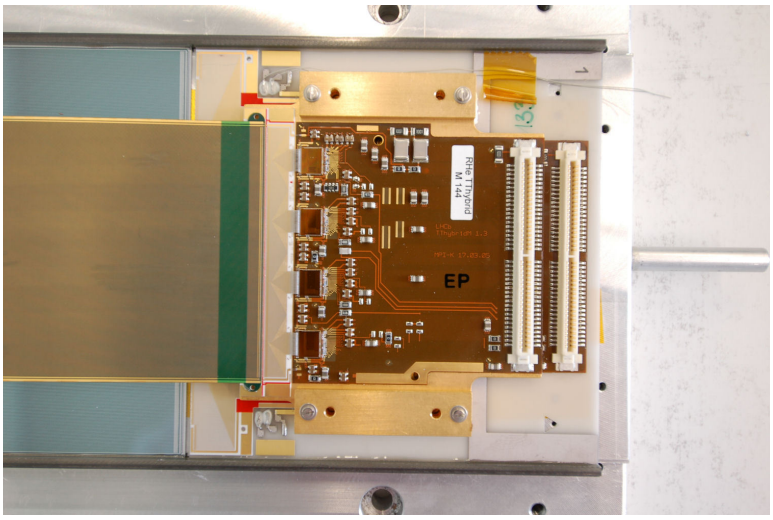

Figure 1.4: This picture shows an M hybrid with four Beetle chips mounted on a module. Each readout channel of the Beetle is connected via wire bonds to the pitch adapter. The pitch adapter is then connected by bonds to either a Kapton cable in case of an M or K hybrid or directly to the first silicon sensor of the L readout sector.

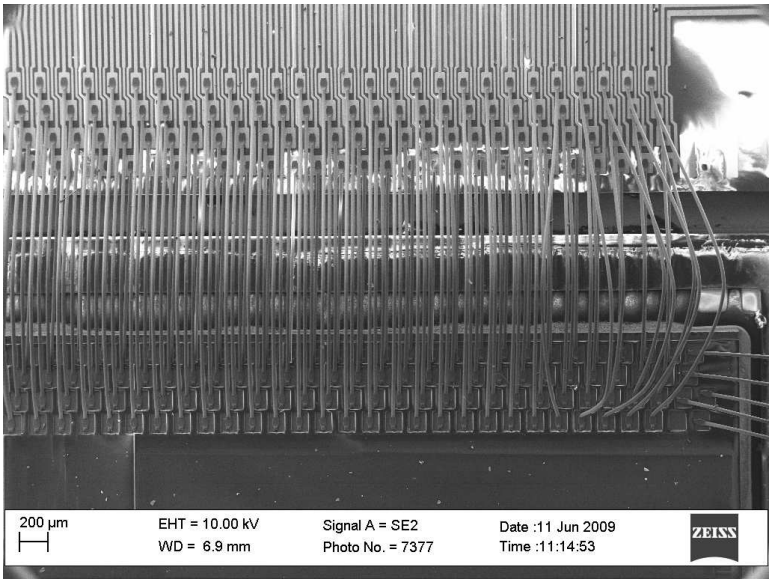

Figure 1.5: This picture shows the four layers of bond wires between the pitch adapter and the Beetle on the M hybrid of module TT 175. On both the Beetle and the pitch adapter side are four rows of bond-pads located. Note that during the disassembling and handling of this hybrid the bond wires on the right have become slightly disordered.

Sector type	Sectors	Beetles	Ports	Strips
L	128	512	2048	65536
M3	104	416	1664	53248
M2	24	96	384	12288
K	24	96	384	12288
TT	280	1120	4480	143360

Table 1.1: Number of readout devices per readout sector type and overall sum in TT.

1.2.1 Signal Generation and Data Acquisition

Signal Generation on a Silicon Micro Strip

The silicon micro-strip sensor in TT consists of 512 diodes on a surface of 9.64 cm by 9.44 cm. The sensor is 500 μm thick and provides an n-doped silicon bulk shared by all the diodes. On top of the sensor, 512 p-doped silicon strips are implanted as shown in Figure 1.6. An AC-coupling of the readout circuit to the p-doped silicon strip is needed to protect the readout circuit from leakage currents through the silicon bulk. Therefore, an insulating layer of $Si0_2$ covers the p-implants. On top of the insulating layer aluminium strips with the same pitch as the p-implants are connected to the readout electronics. On the bottom of the sensor there is an n^+ doped backplane

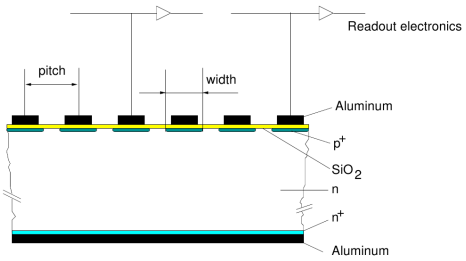

Figure 1.6: The layout of a silicon micro-strip detector [2].

and an aluminium layer allowing to apply a positive reverse bias voltage and fully deplete the silicon bulk. When hit by an ionising particle, electron-hole pairs are created along the track of the particle. Due to the electrical field of the bias voltage the electrons and holes are accelerated and lead to a current in the reverse direction of the bias voltage. The strip pitch on the sensor of 183 μm allows track reconstruction of charged particles within the required precision of $\pm 50\,\mu$m. The signal collection time is about 20 ns allowing high-rate data acquisition.

The Beetle

Signals generated on the silicon strips are read out via the hybrid. On the hybrid there are four readout chips, called Beetles.

A Beetle integrates 128 channels. The signal is pre-amplified and shaped. The pulse shape, i.e the peaking time and the remainder after 25 ns can be set via the v_{fs} parameter. In addition, there is a pipeline provided to buffer up to 160 signals. Input signals are serialised onto four analogue output ports. Details about the Beetle are mentioned in the text or can be found in Ref. [3].

The Digitiser Board

On the digitiser board the analogue signals sent by the Beetle through its four output lines are converted into digital signals. The signal height then is expressed in Analog-to-Digital-Converter (ADC) counts. Digital signals from the four beetle output lines are serialised into one optical transmission line to the TELL1 board.

The TELL1 Board

The TELL1 board contains FPGAs which perform the following data processing steps.

Pedestal Subtraction: The average signal height is determined for each channel and subtracted from the actual signal height.

Common Mode Subtraction: Like an antenna, the readout strip is sensitive to electromagnetic fields in the area. Due to the fact that these fields are neither static nor homogenous, the signal height on the strips is subject to a shift. Neighbouring strips are shifted by a similar amount. It is called the common mode and changes from event to event. The common mode of signals is determined for each port and removed by the common mode subtraction (CMS) algorithm.

Cluster Finding: If data is recorded, this happens for all the strips of the TT detector in the same moment, no matter if a particle has passed by or not. As the occupancy is rather low for the TT detector, on most of the strips only noise signals are recorded. Charged particles passing through the TT detector create signals on more than one neighbouring strip of the sensor and form a cluster of signals. On the TELL1 board an algorithm is implemented to detect signal clusters.

Zero Suppression: In order to reduce the amount of data, zero suppression (ZS) dumps all data that is not part of a cluster. If zero suppression is not enabled, data is taken in the non zero suppressed (NZS) mode and all data recorded is kept for further processing and analyses.

There are 48 TELL1 boards performing these data processing steps for 3072 readout channels each. The TELL1 boards are labeled with the TELL1 No. $1, 2, \ldots, 48$ which will be referred to within this text[1]. For the complete list of tasks and more details see Ref. [4].

Strips and channels

There are 143360 silicon readout strips within the TT. Each type of readout device, e.g. a Beetle readout chip, has a certain number of readout channels N_{d}. The number of readout channels per device is listed in Table 1.2.

Device	N_d
TELL1	3072
Sector	512
Beetle	128
Port	32

Table 1.2: Number of readout channels N_d per readout device type.

1.2.2 Noise

When operated in NZS mode, the readout electronics registers an ADC value for each channel even when no particle hits a strip. For a given channel and with many measurements without hits, a distribution of ADC values is recorded as the output is not always exactly the same. The mean of this distribution is called the pedestal and the rms is called the noise of the channel.

A prediction of the noise in silicon micro strip detectors connected to the Beetle is elaborated in detail Ref. [5]. According to this note, the equivalent noise charge (ENC) for a RCCR filter with only one filter step is

$$\mathrm{ENC}^2 = \frac{e^2}{8\tau} \times \frac{8kT}{3g_m} \cdot C^2 + \frac{e^2 \cdot \tau}{8} \cdot 2q_e \cdot I,$$

where I is the leakage current in the sensor, τ is the shaping time of the Beetle, e is Euler's number and q_e is the charge of the electron, k is the Boltzmann-constant, T is the temperature and g_m is the transconductance. As the Beetle v.1.3 implemented in the TT detector is quite different from a first order RCCR filter considered to derive the formula given, it should not be used for exact noise predictions. However, the ENC^2 is proportional to the capacitance C^2 of the strip and the leakage current I on the sensor. A large noise is expected due to the large capacitance of the strips and the

[1] In fact, a second nonconsecutive numbering of the TELL1 boards, called the sourceID, is in use. Within this text only the TELL1 No. will be given.

short shaping time that is needed to be able to read out data at a frequency of up to 40 MHz. In addition, radiation damage on the sensors could enhance the leakage current in future and rise the noise.

The signal heigth is limited by the detector thickness that in particular is restricted by the drift time of the electron-holes to the p doped readout strip. Due to the limited signal and quite high noise on the long strips in TT, the signal-to-noise ratio is rather small[2]. For instance, the smallest expected signal-to-noise performance in the TT detector is approximately $S/N \sim 13$, for strips of an M3 readout sector with V_{fs} =400 mV [11]. Having a signal-to-noise ratio below 10 would make hit detection with reasonable efficiency and purity a very challenging task [6]. Therefore, a good understanding of the noise on TT silicon strips is important.

Furthermore, when searching for low noise channels (see Chapter 3), one would like to have a noise that is well-understood and rather stable.

[2]For comparison, the VELO, which has much shorter strips than the TT detector, expects a signal-to-noise ratio between 21 and 30 [7].

Chapter 2

Noise Calculation

In this chapter studies of the noise calculation will be described. In addition, a phenomenon related to the pipeline column number (PCN) will be covered.

The current understanding of the noise in the TT detector was incomplete due to a limited knowledge of the effect of the header cross talk and the influence of the PCN on the pedestals. The noise calculation was modified to study these effects and improve the calculation of the noise. In the following sections the development of the modification on the noise calculation will be described.

The data sets taken into account for the work done within this thesis are listed in Table 2.1. For consistency, only data sets having the same properties were taken into account, e.g. high voltage settings of 250 V. When comparing noise values of different runs, the noise has been calculated based on 4010 events. All the data was recorded in NZS mode, shaping time parameter $V_{fs} = 400$ and without testpulses.

2.1 The Header and Header Cross Talk

As mentioned in Section 1.2.1, there is a pipeline for each readout channel in the Beetle chip. After integrating, shaping and sampling of the signal generated on the strip, its height is buffered in the pipeline. The signal height is stored in a pipeline cell at the rate of the LHC bunch crossing frequency of 40 MHz. The pipeline can store 160 consecutively sampled signals. This is needed to keep the signal buffered until the level zero trigger system has decided whether it is part of an interesting physical event and has to be kept for further processing. In addition the pipeline requires some more cells for internal bookkeeping and contains a total of 187 cells. Pipeline cells are numbered in order to synchronise signals recorded on Beetles all over the TT detector.

Run	LHCb run No.	Date	Number of events
0	35605	17 October 2008	20000
1	43225	30 January 2009	4010
2	44288	19 February 2009	5000
3	46054	19 March 2009	5000
4	46819	31 March 2009	5000
5	48435	22 April 2009	4010
6	50024	3 June 2009	5000
7	50038	3 June 2009	5000
8	51737	30 June 2009	5000
9	52076	3 July 2009	10000

Table 2.1: List of runs taken into account to create history of noise values and search for possible (soft and hard) cuts. The run numbering in the first column is arbitrary and used as an alias in plots where the noise is given as a function of the run number. The data was recorded with a bias voltage of 250 V in NZS mode, $V_{fs} = 400$ and without test-pulses.

2.1.1 The Header

The analogue signal of 128 parallel input channels are multiplexed onto four output ports, i.e. transformed into $4times32$ consecutive analogue signals. In order to keep track of the time when the input signals were recorded, the PCN is assigned and shipped with the data set to the next processing unit[1]. Therefore, each data set is preceeded by a header containing the PCN and further information. The header consists of four analogue signals per port. Figure 2.1 shows the distributed encoding of the eight bit PCN in the header of the four ports of the Beetle. Header bit three of the port 0 encodes the least significant bit (LSB) P0 of the PCN. To determine whether the PCN is even or odd, one only has to check if P0 is either low (0) or high (1) respectively.

For the ST system the first header bit is not used. The second header bit is always low. Thus, only header bits two and three can be either high or low and the four different configurations listed in Table 2.2 can occur in the header.

On port three, there are only three header configurations as the highest number to be encoded using 8 binary bits is 255. However, there are only 187 pipeline cells. Therefore the configuration where both bits are high (11) does not occur in the header of port 3 where P7 and P6 are encoded.

[1] All channels of TT are read out at the same time. The entire of the recorded signals makes an event. The pipeline column number (PCN) serves as a timestamp and links the recorded signal to the event.

header bit				configuration
0	1	2	3	name
-	low	low	low	00
-	low	low	high	01
-	low	high	low	10
-	low	high	high	11

Table 2.2: The Beetle header configurations. Header bit-0 is not transmitted and bit-1 is always set to low. Therefore, four different header configurations are possible, except for port three where configuration 11 does not occur due to the limited number of pipeline cells.

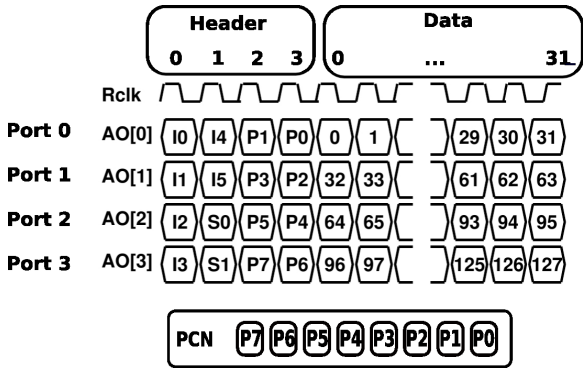

Figure 2.1: When operating the Beetle in analogue readout mode, 1×128 analogue input signals are multiplexed in 4×32 analogue output signals on four ports with up to 40 MHz. This Figure shows the schema of information transmitted. Signals at labels preceded by I, P or S belong to the header. Bits encoding the PCN are labelled P0 to P7. The LSB P0 determines whether the PCN is even or odd. Sampled input signals are labelled 0–127. Original picture from Ref. [3].

2.1.2 Header Cross Talk

Within the Beetle, there is cross talk between the last header bit and the signal of the first channel of a port. For example, there is cross talk form header bit P2 to signal 32, according to the layout describing the serialising of signals shown in Figure 2.1. This cross talk is referred to as the header cross talk and is investigated in e.g. Ref. [8]. Header cross talk causes a shift of the signal height recorded on the strip connected to the first channel of a port.

In data acquisition, the header cross talk is corrected by changing the signal height by a fixed amount depending on whether the last header bit is either high or low. This so-called header corrections should remove the cross talk to avoid problems in further data processing.

2.2 Header Cross Talk in the Raw Noise

In Figure 2.2, an example of a typical raw noise pattern is shown. Clearly visible are the large spikes which occur regularly on the first few strips of a readout port. This effect is related to the header cross talk on the Beetle chip which is not corrected for in raw data. Consider the first channel of a port. There is a shift of the analogue signal in the first channel of a port, due to header cross talk. As the shift of the signal depends on whether the preceding header is high or low, the spread of the distribution of signal heights increases. The noise of this channel therefore is expected to be higher than on a channel which is not affected by cross talk.

However, considering header cross talk as it is understood, one would expect a higher noise only on the first channel of each port. The noise pattern though shows a peak on the first few channels. This is not understood and under investigation.

Currently higher-order header corrections, e.g. to correct for a cross talk of the last header bit onto the second channel, the second last header bit onto the first channel, are under investigation.

In addition, corrections based on the difference between the signal height of the header bit and the readout channel are studied [9].

To remove the effect of the header cross talk on the noise, the noise calculation was modified in order to take the header configuration into account. This is explained in detail in the following section.

2.3 Using the Header Configuration in the Calculation of the Noise

Consider a given readout channel: The shift of the recorded signal height depends on the header. As described in Section 2.1.1 the header changes, but

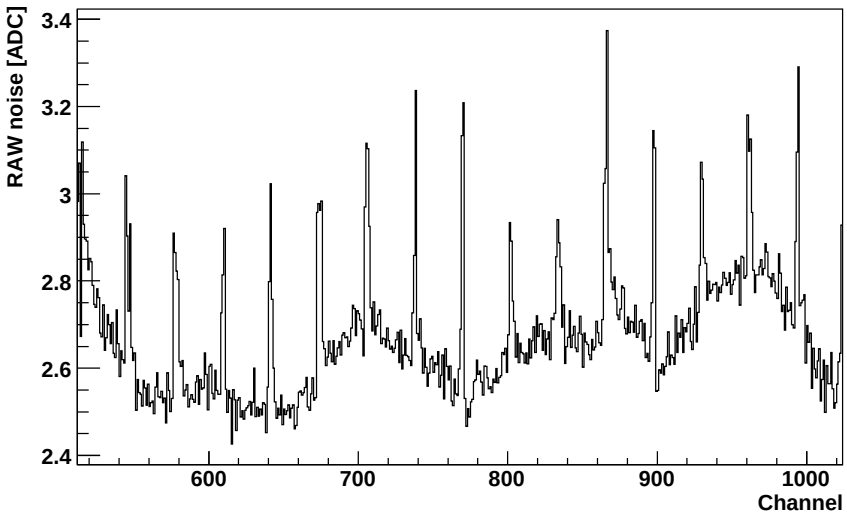

Figure 2.2: The raw noise determined with the default noise computation for the readout channels 512 to 1023 of TELL1 No. 17 corresponding to an L sector on TTx1 Layer. Clearly visible are the large spikes regularly occurring on the first few strips on each port, i.e. every 32 readout channels. This effect is related to the internal cross talk on the Beetle. Data is from run 50038.

only four header configurations can occur. For a fixed header configuration the shift of the signal height is constant. Therefore, a noise calculation based on signals preceeded by a header of a given configurtation only is not sensitive to the header cross talk. The pedestal determined with this subset of signals is shifted only. In order not to loose any data, a noise calculation taking all header configurations (the header is also available offline) into account has been implemented as follows. Determine the noise n on this channel based on a set of n ADC values as:

1. Split the data set into four subsets where only ADC values preceded by the same header configuration are contained.
2. Determine the spread for each subset

$$rms_{00}, rms_{01}, rms_{10}, rms_{11}.$$

3. Calculate the noise of the strip as a weighted average of the spreads:

$$n = \frac{rms_{00} \times N_{00} + rms_{01} \times N_{01} + rms_{10} \times N_{10} + rms_{11} \times N_{11}}{N},$$

where N_{ij} is the number of ADC values in the subset.

In Fig. 2.3 the result of the noise calculation taking the header configurations into account is compared to the default noise calculation for 512

readout channels on one of the TELL1 boards. One can clearly see that the effect of the header cross talk is suppressed. Surprising however is the fact that the noise on channels corresponding to port zero of each Beetle is significantly lower. This drop in noise is related to the fact that the pedestal height depends on the PCN parity. This effect is investigated in more detail within the following section.

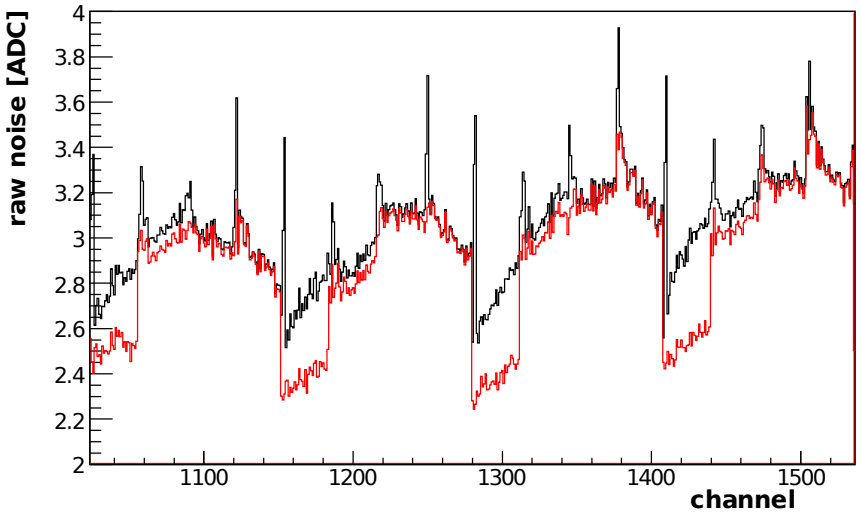

Figure 2.3: The noise on channels 1024 to 1535 on one of the TELL1 boards is shown[2]. The noise was calculated using the default noise calculation (black) and taking the four header configurations into account (red). Cross talk effects from the header on the noise are suppressed. More surprising is the fact that noise on the channels of port zero are significantly lower. Data is from run 48435.

2.4 Pedestal Shift

In the previous section it was shown that the cross talk causes a shift of the pedestals calculated on the first few channels of a port and that the shift depends on the header configuration. An additional pedestal shift has been found, where pedestals of any channel within a readout sector are subject to a shift which is dependent on the PCN. Figure 2.4 shows that if the PCN is odd, the pedestal of a given strip is up to about five ADC values higher than the pedestal when the PCN is even. This shift is not understood and needs further investigation.

[2]The plot shown in Figure 2.3 shows the noise pattern on channels 1024–1535 of TELL1 No. 1.

Figure 2.5 shows the the difference $\Delta\overline{p}$ as a function of the channel number for the four different readout sector types. Note that the difference $\Delta\overline{p}$ is computed using average pedestals $\overline{p}$. To calculate the average pedestal, consider a readout sector type (e.g. L) and a channel number (e.g. 5). E.g. averaged are the pedestals of each readout channel No. 5 of the 128 L-type readout sectors. The difference between average PCN-odd and average PCN-even pedestals on M3, M2 and K sectors is larger than for L sectors and rises slightly toward higher channel numbers. The difference increases towards the middle of the Beetle. At the edge of each port, there is a small spike.

Figure 2.6 shows the distribution of the difference $\Delta p = p_{odd} - p_{even}$ (determined for each readout channel separately) for the four readout sector types. To provide an overview the mean difference and the rms of the distribution is listed in Table 2.3 for each readout sector type.

In Figures reffig:PedDiff-LMK–2.8 the difference Δp between PCN-odd and even pedestals is calculated for each readout strip seperately.

In the distribution of Δp for K type sectors in Figure 2.6, there is a small peak around zero. This peak is caused by a single readout sector (sector 3 of TELL1 No. 15) as illustrated in Figure 2.7.

sector type	mean [ADC]	rms [ADC]
L	0.44	1.0
M3	4.54	0.9
M2	4.59	0.7
K	3.18	1.0

Table 2.3: Mean and rms of the distribution of $\Delta p = p_{odd} - p_{even}$ for the different types of readout sectors, see Figure 2.6. Data of run 51978 is used.

In Figure 2.8 the distribution of Δp for Beetle 0 has a significant lower mean than the distributions of Beetles 1, 2 and 3 for L type sectors. In addition the distributions of the Beetles on L type sectors have larger tails on the left-hand side, compared to similar distributions drawn for the other sector types.

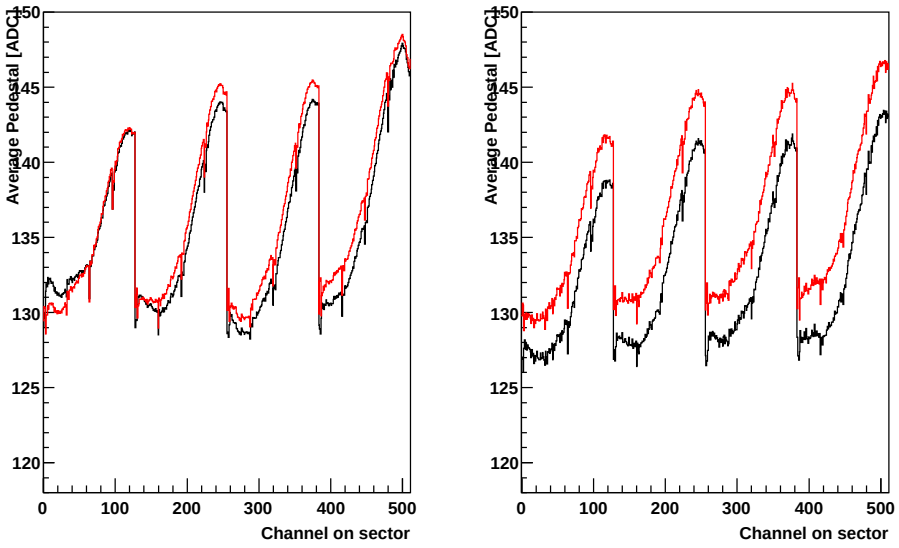

(a) L type readout sectors (left) and K type readout sectors (right).

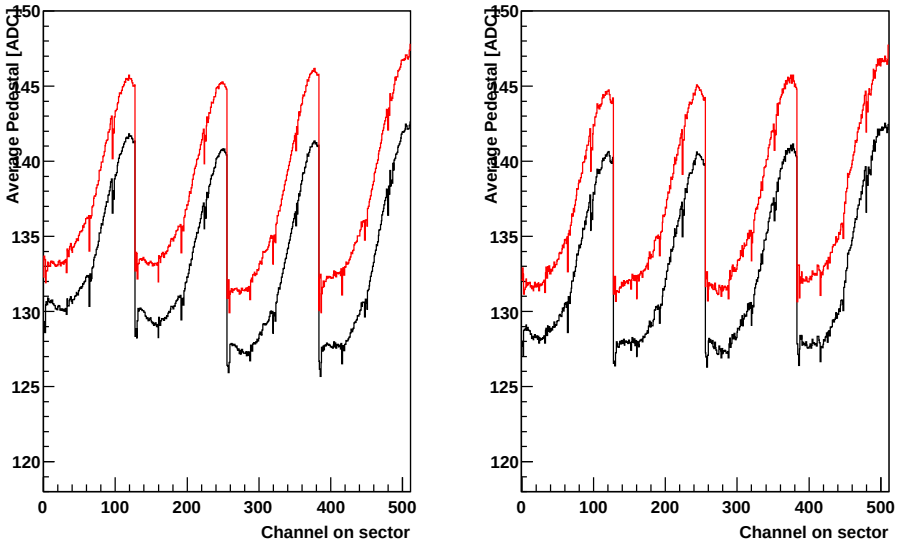

(b) M3 type readout sectors (left) and M2 type readout sectors (right).

Figure 2.4: Average pedestals as a function of the channel for the four types of readout sectors. The average pedestal calculated for odd PCN numbers is drawn in red, and the one for even PCN numbers in black. To calculate the average pedestal, consider a readout sector type (e.g. L) and a channel number (e.g. 5). E.g. averaged are the pedestals of each readout channel No. 5 of the 128 L-type readout sectors. Run from run 51978.

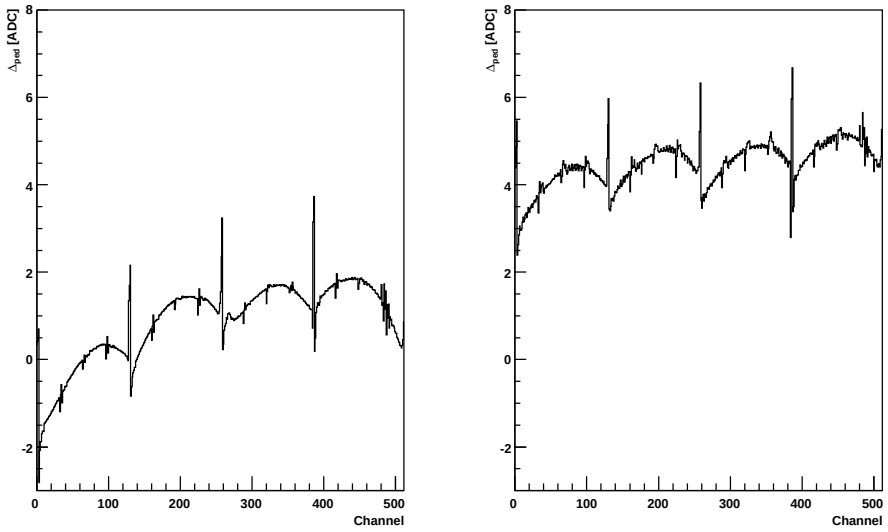

(a) L type readout sectors (left) and K type readout sectors (right).

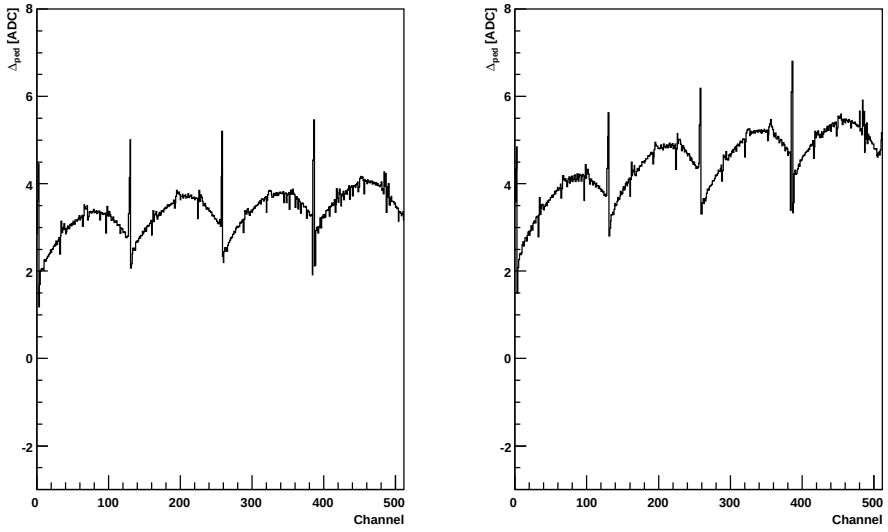

(b) M3 type readout sectors (left) and M2 type readout sectors (right).

Figure 2.5: The difference $\Delta\overline{p} = \overline{p}_{odd} - \overline{p}_{even}$ between average even pedestals and average odd pedestals is drawn as a function of the channel number for each type of readout sectors. To calculate the average pedestal, consider a readout sector type (e.g. L) and a channel number (e.g. 5). E.g. averaged are the pedestals of each readout channel No. 5 of the 128 L-type readout sectors. Data is from run 51978.

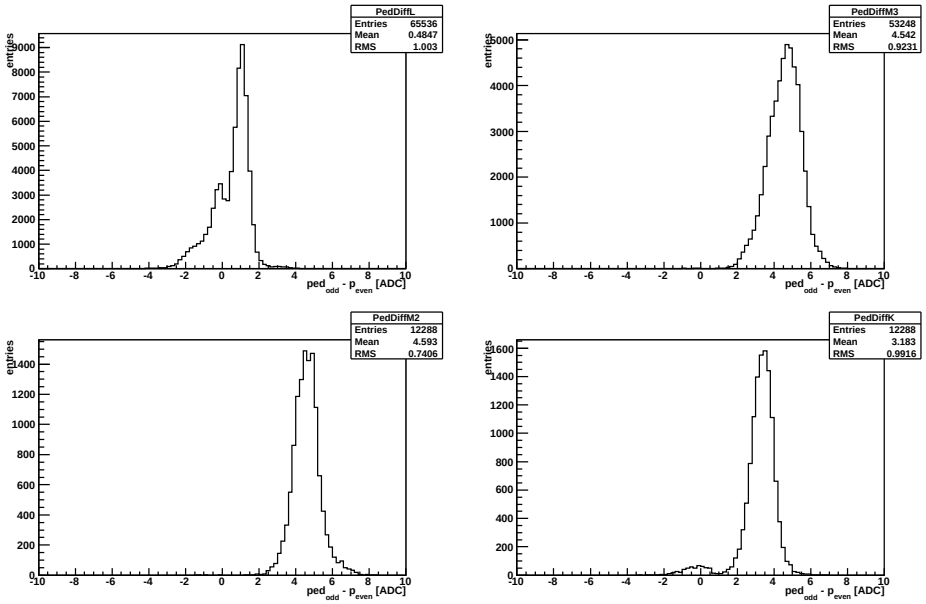

Figure 2.6: This are the distributions of the difference $\Delta p = p_{odd} - p_{even}$ (determined for each readout strip) for each type of readout sector. Data from run 51978.

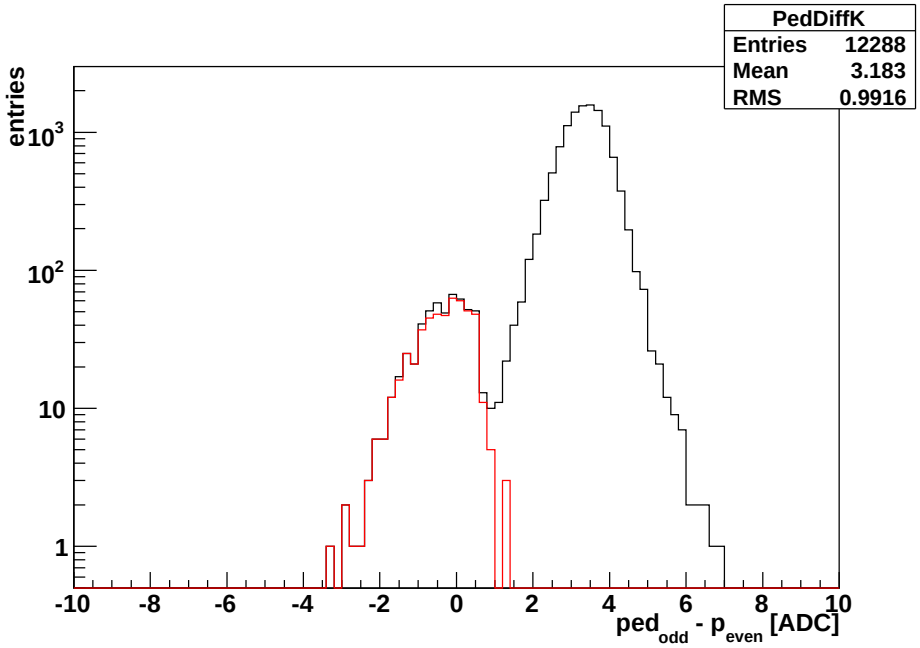

Figure 2.7: The distribution drawn in black shows the difference $\Delta p = p_{odd} - p_{even}$ calculated for short strips of K readout sectors. In red the distribution of Δp for the readout sector 3 of TELL1 No. 15 is drawn. Data is from run 51978.

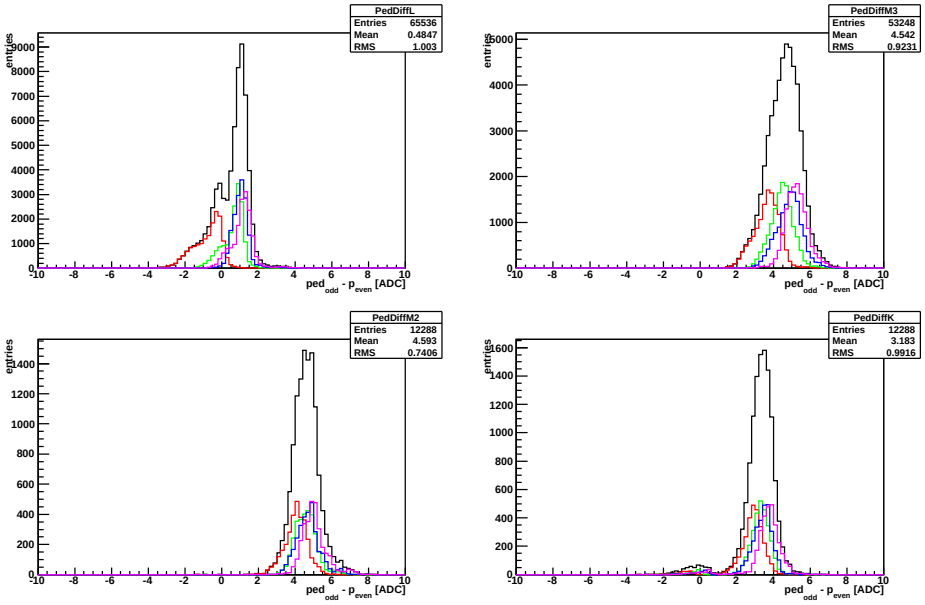

Figure 2.8: The distributions of the difference $\Delta p = p_{odd} - p_{even}$ (determined for each strip) for the different types of readout sectors are drawn in black. The distributions for a given subset of strips are drawn in colour: channels 0 – 127 (Beetle 0) of the corresponding readout sector, red; channels 128 – 255 (Beetle 1), green; channels 256 – 383 (Beetle 2), blue; channels 384 – 512 (Beetle 3), pink. Remark the offset for channels 0 – 127 on the L readout sectors. Data is from run 51978.

2.5 Taking Pedestal shifts into Account for the Noise Calculation

As described in Section 2.3 the noise for a given strip is calculated on a set N ADC values. To take the pedestal shift into account the calculation was modified as follows:

1. The data set was split into eight subsets, one for each header configuration and with the PCN even or odd:

   $$A_{00\ \text{even}}, A_{00\ \text{odd}}, \ldots, A_{11\ \text{odd}}.$$

   An exception exists from data recorded on strips connected to a port zero of the Beetle. The bits P0 and P1 of the PCN are encoded here, therefore the four header configurations already take into account whether the PCN is even or odd. Subsets

   $$A_{00\ \text{even}}, A_{01\ \text{odd}}, A_{10\ \text{odd}}, A_{11\ \text{even}}$$

   therefore do not exist for port zero.
2. The spread $rms_{ij,\ \text{even (odd)}}$ for each subset of ADC values was determined.
3. The noise was calculated as a weighted average of the spreads:

   $$\text{noise} = \frac{rms_{00\ \text{even}} \times N_{00\ \text{even}} + \ldots + rms_{11\ \text{odd}} \times N_{11\ \text{odd}}}{N},$$

   where $N_{ij,\ \text{even|odd}}$ is the number of ADC values contained in a given subset. This will be referred to as the modified noise calculation method and was used in all the plots, unless stated to be different.

2.6 Noise Distributions

In the following section various noise distributions will be shown. In Figure 2.9 the noise distribution for all readout strips of the TT detector is shown. There is a large, broad peak at 2.7 ADC and rather flat tails to the right (low noise) and left (high noise). The steep edge to the left at 2 ADC will allow to place a cut to define low noise channels. This will be described in Section 3.1. The little peak around 1 ADC is mainly due to recently broken bond wires. A cut to define high noise channels was not investigated. For documentation, channels with a noise higher than 4 ADC values in a particular measurement are listed in Table A.1 in the Appendix.

The broad shape of the peak at 2.7 ADC is due to the noise distributions drawn for the different types of readout sectors as illustrated in Figure 2.10. One expects shifted mean values of the noise distributions for the four types of readout sectors due to different strip and cable lengths.

Using a test beam, the equivalent noise charge (ENC) of a readout channel was measured to be

$$\mathrm{ENC} = 776\,[\mathrm{e}^-] + 47.9\,[\mathrm{e}^-/\mathrm{pF}] \times C[\mathrm{pf}]$$

(The test was performed with Beetle v. 1.2, $V_{fs} = 400\,\mathrm{mV}$ [10]). For a given readout sector the strip length, the total strip capacitance including the Kapton cable and the expected ENC according to the test beam measurements are given in Table 2.4.

sector type		l_{strip} [cm]	l_{cable} [cm]	C [pF]	ENC [e^-]
L:	4 sensors	37.76	-	54.9	3405.7
M3:	3 sensors + cable	28.32	39.1	57.3	3520.7
M2:	2 sensors + cable	18.88	39.1	44.1	2888.4
K:	1 sensor + cable	9.44	58.0	38.4	2615.4

Table 2.4: Strip and Kapton cable length, total strip capacitances C including capacities of both strip and Kapton cable and expected equivalent noise charge (ENC) according to test beam measurements for TT readout sector types [10][11].

In Figure 2.10 the noise distributions for strips of the different types of readout sectors are shown. The noise was computed with the modified method. The mean of the noise distributions and the expected ENC for channels of a given sector type are compared in Table 2.5. Note that the M3 type readout sector has highest mean noise as expected according to the determined ENC. In contradiction to the expectation, the mean noise of L readout sector is lower than for K and M2 readout sectors.

Drawing the distribution for the difference $n_{mod.calc.} - n_{def.calc.}$ of the noise calculated for each strips of readout strip by the modified and default methods respectively, one obtains no entries above zero as can be seen in

sector type	mean [ADC]	rms [ADC]	expected ENC [e^-]
M3	3.013	0.1968	3520.7
L	2.477	0.1181	3405.7
M2	2.809	0.1659	2888.4
K	2.733	0.1482	2615.4

Table 2.5: Mean and rms of the noise distributions for the readout sector types shown in Figure 2.10. The expected ENC according to the test beam measurements is given in the last column (See also Table 2.4).

Figure 2.11. Applying the modified noise calculation therefore results in a decrease of noise throughout the detector.

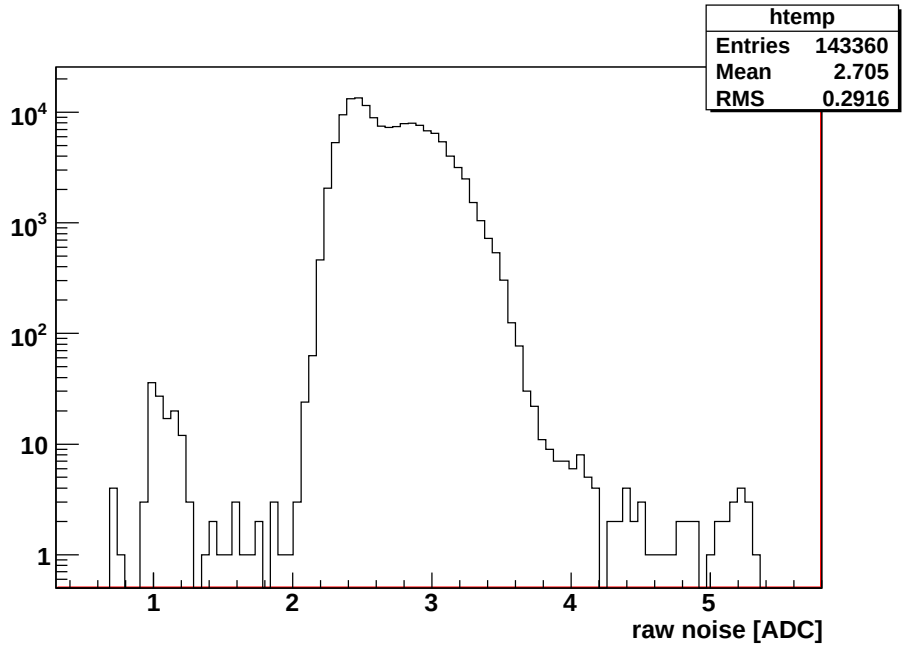

Figure 2.9: Noise distribution for all strips of the TT detector of data recorded in run 52076. Open channels and broken bonds peak at 1 ADC. Channels having noise higher than 4 ADC values are listed in Table A.1. The same plot without logarithmic y axis is shown in Figure A.2. Noise was calculated with the modified method.

[3]Within the DAQ-Software, the conditions database keeps status information of the detector. For each readout strip, tags can be set according to the problem the strip is affected. In case the strip status is OK, no known problem is reported and the strip is fully funtional.

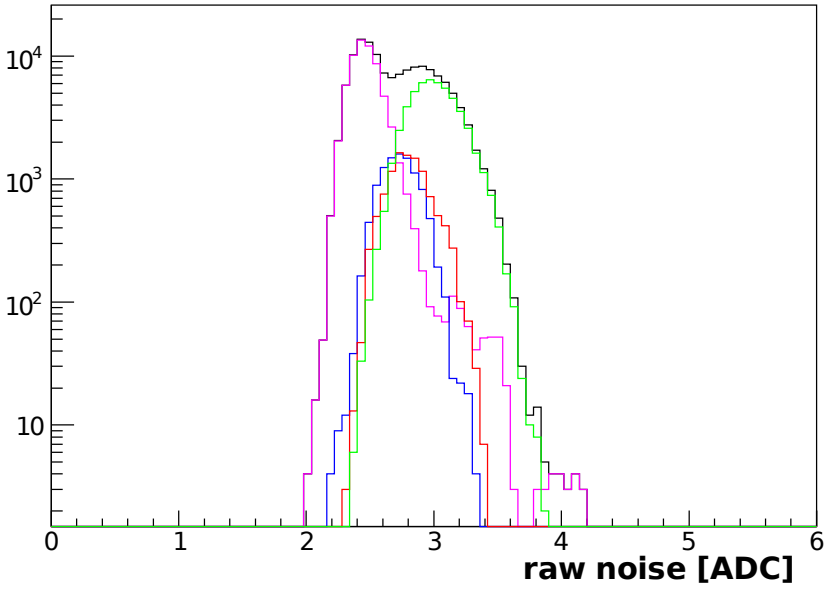

Figure 2.10: Noise distribution of all strips (black), strips of L type sectors (pink), strips of M2 type sectors (red), strips of M3 type sectors (green), strips of K type sectors (blue). Noise calculated with the modified method. Low noise channels, i.e. $n < 1.75$ADC, channels having any other strip status than OK[3] and the first and the last channel of the readout sector (possible pickup noise) were not taken in to account when drawing the distributions in order to exclude known problems. Data is from run 51737. The same plot without logarithmic y-axis is shown in Figure A.2.

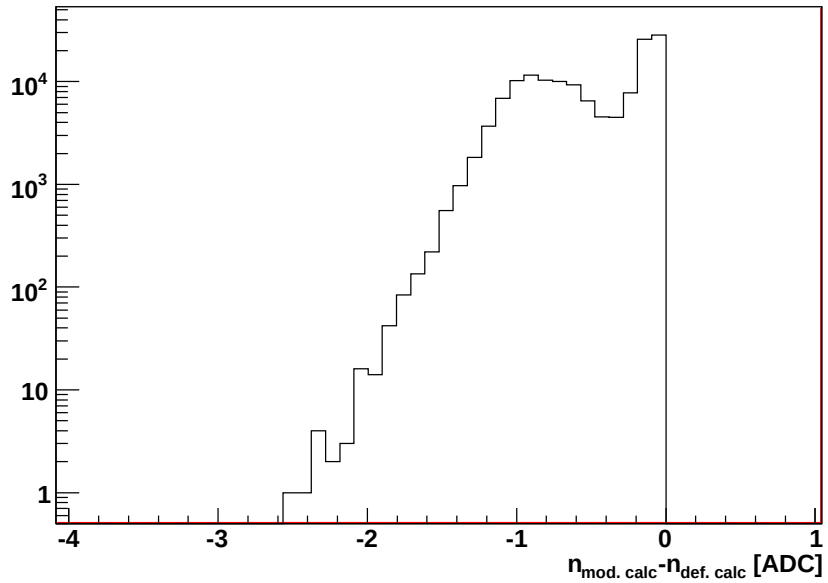

Figure 2.11: Distribution of the difference $n_{mod.calc.} - n_{def.calc.}$ of the noise calculated for each readout strip by the modified and default methods respectively. There are no entries above zero. As expected, the noise is smaller when computed with the modified method. Data is from run 52076.

2.7 Average Noise as a Function of the Channel Number

Figure 2.12 shows the comparison of the default and the modified noise calculation. For each sector type, the average noise on the channel is drawn as a function of the channel number. The effect of the header cross talk on the noise is widely suppressed. Except for the L type sectors, there is quite a big decrease in raw noise when computed with the modified method.

In Figure 2.13 the noise for the different sector types are shown in one plot for the default noise calculation. For the modified noise calculation the plot is given in Figure 2.14. As mentioned before, the L type sectors have lowest noise in both of the Figures 2.13 and 2.14 against the expectation according to the test beam measurements.

In Figures 2.15–2.17 the average noise is given as a funtion of the channel number of the readout port (0–31). To calculate the average noise on the port, consider a channel number, e.g. 5 (and a sector type): averaged are the noise values of readout channel No. 5 of each port (of the selected sector type).

In Figure 2.15 the two noise computation methods are compared. Again the effect of the cross talk on the noise is visible when using the default noise calculation and inhibited by the modified noise calculation. Note that the average noise on the first strip is lower compared to second and third strip for the default calculation. This was not further investigated.

Figure 2.16 shows the average noise for the different readout sectors determined using the modified computation. The L sector shows again lowest average noise as described in Figures 2.13 and 2.13.

A guard ring around the module was designed shield the readout strips on the edges of a readout sector, e.g. strips 0 and 511, from inhomogeneous electromagnetic fields at the edgedes of the sensor[4]. In order to investigate pickup noise on the outer readout strips, the first and last five strips of the readout sectors were not taken into account to calculate the average noise as a function of the channel number on the readout port, as shown in Figure 2.17 in red. For comparison, the average noise as a function of the channel number on the readout port without any further restriction is drawn in black in the same plots. In case of pickup noise due to depleation field (and the high-voltage needed to create this) one expects lower average when noise data of strips on the edge of the sensor is excluded. I notice that the L type sectors might show this effect. Wheter the decrease in average noise due to excluding strip possibly exposed to pickup noise is significant on the

[4]To depleate the silicon bulk a reverse bias voltage is applied to the sensor in order to create a homogeneous electric field in the sensor. However, on the edges of a charged plate, there always are inhomogenites in the electric field which can lead to pickup noise in the outer readout strips. The guard ring is designed to cope with these inhomogenities and to reduce pickup noise on the outer channels.

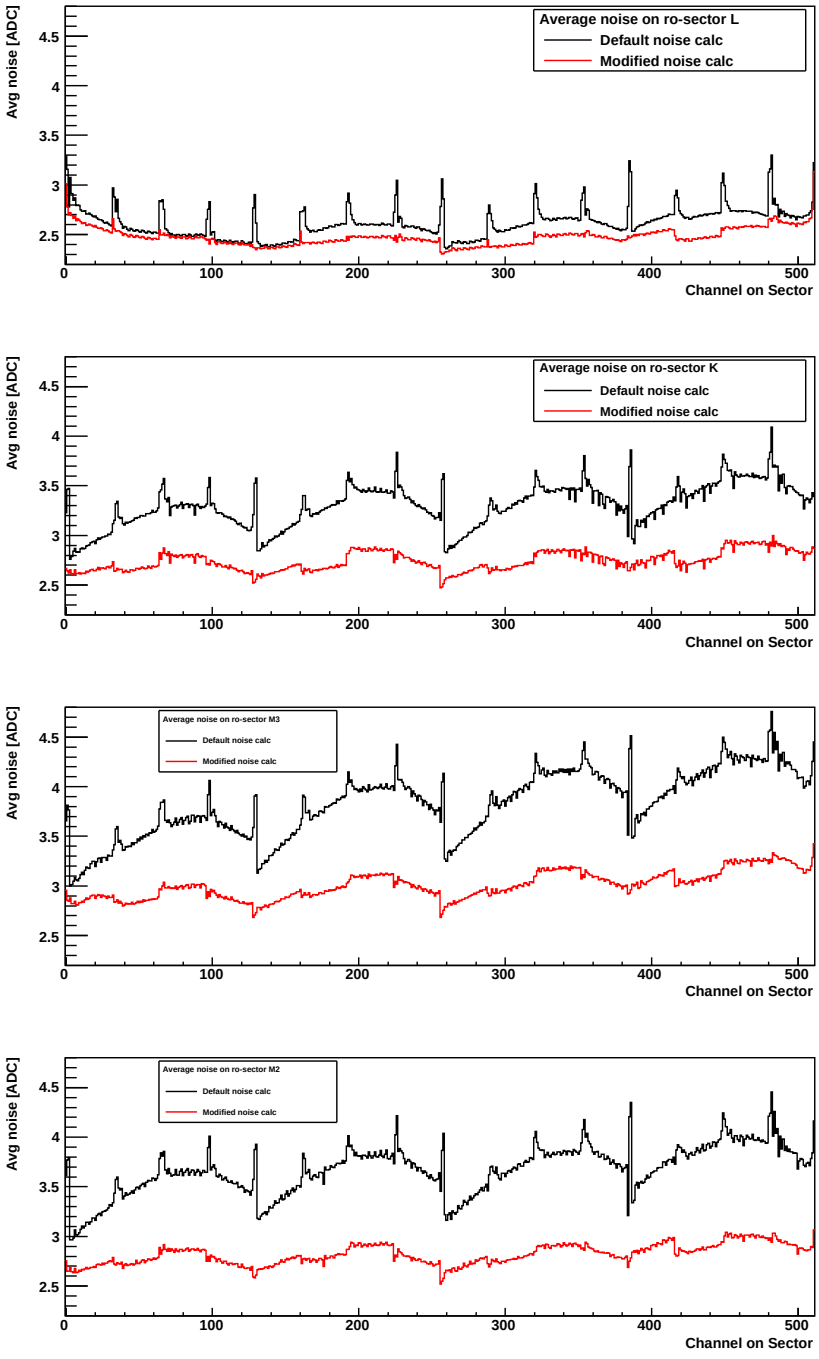

Figure 2.12: The plots show the noise versus channel number (0–511) averaged over all readout sectors of a given type. The two different methods to calculated the noise are compared. Data is from run 51737.

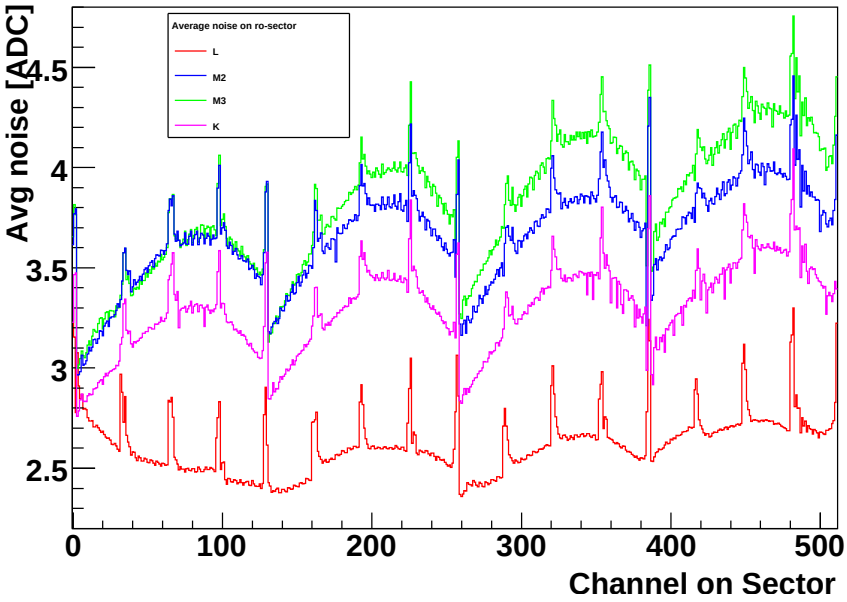

Figure 2.13: This plot shows the noise levels for each type of readout sector versus channel number (0–511). Data is from run 51737.

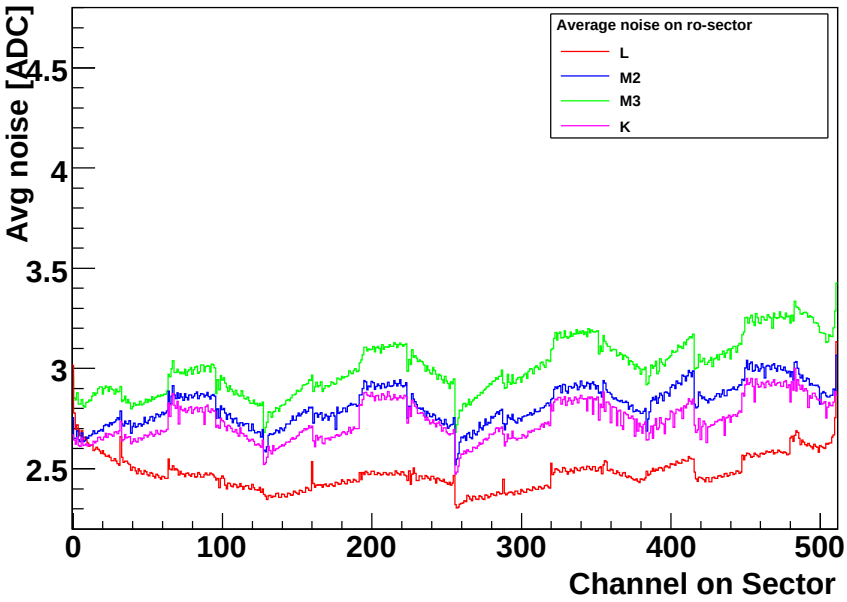

Figure 2.14: The plot shows the noise levels for each different type of readout sector versus channel number (0–511) of the readout sector. Data is from run 51737.

first channels remains to be investigated. However, for the sector types K, M2 and M3 no indication for this effect can be seen according to Figure 2.17.

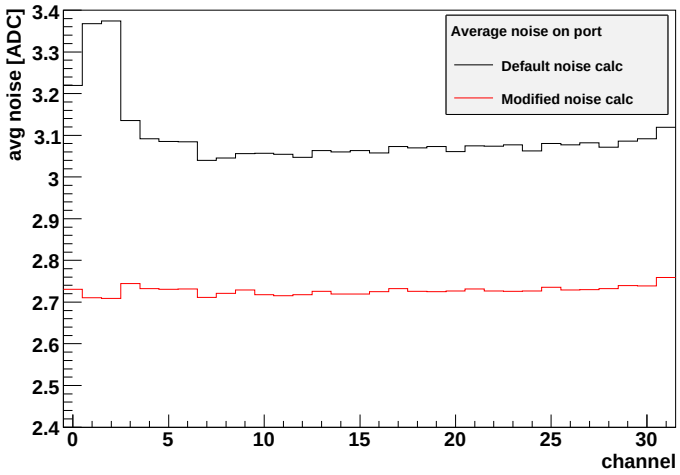

Figure 2.15: The plot shows the noise as a function of the channel number within a readout port averaged over all readout ports based on the default and the modified method. The noise levels are averages of up to 4480 noise values, as one counts a total of 4480 readout ports within the TT detector, see Table 1.1. Data is from run 51737.

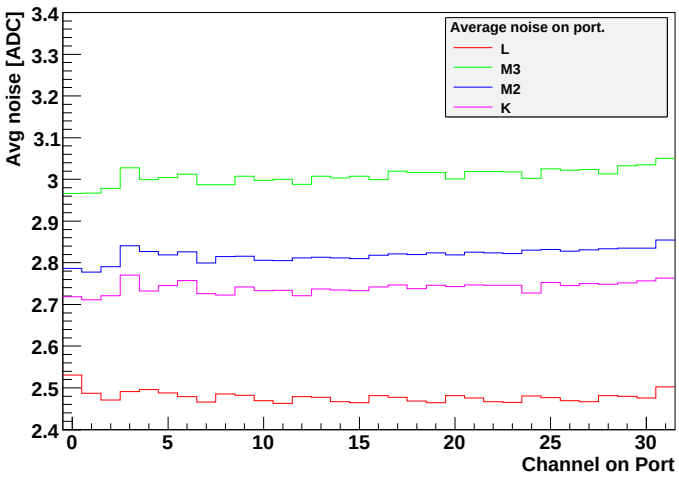

Figure 2.16: For the modified noise computation the noise levels on the readout port were computed also for the each type of readout sector separately. The number of ports belonging to the 4 different types of readout sectors are indicated in Table 1.1. Data is from run 51737.

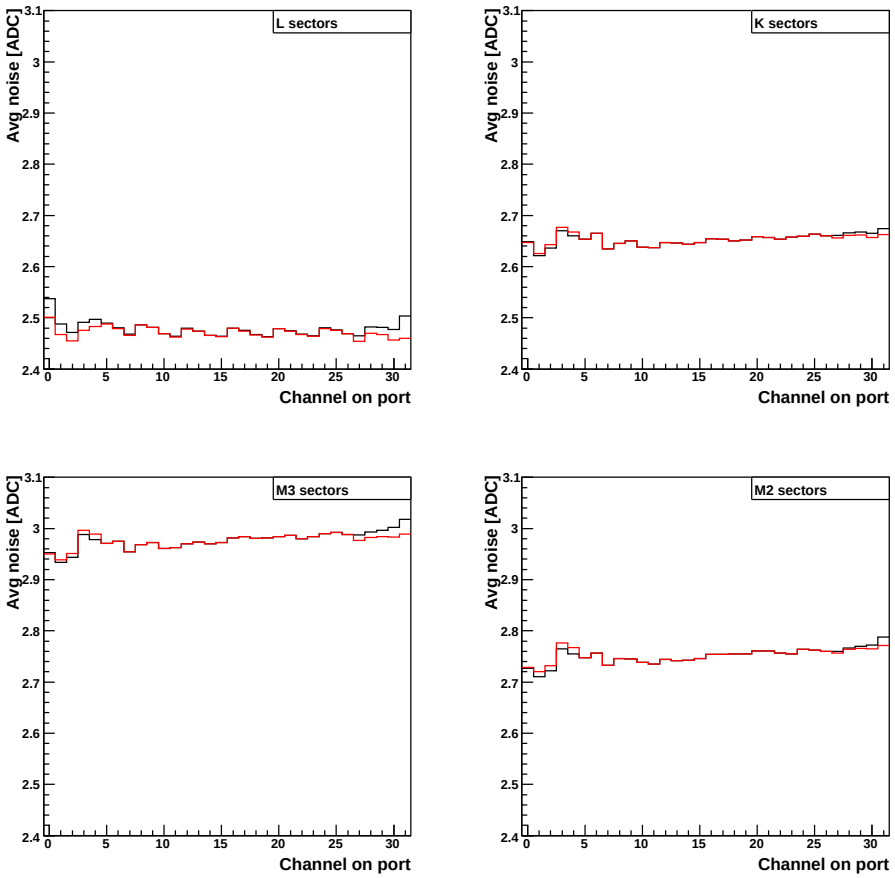

Figure 2.17: Additional noise on the edge of the readout sector is investigated by excluding the first and last 5 strips when calculating the average noise on the port (red). In black the noise level for healthy strips, i.e. StripStatus = OK, is drawn. Data is from run 51737.

Chapter 3

Monitoring Low Noise Channels

Dead readout channels will reduce efficiency and the spatial resolution of the TT detector. Knowledge of dead or faulty channels is therefore important. In particular, one is looking for channels which have low noise. A possible reason for a lower noise are broken electrical connections anywhere between the Beetle input and the end of the readout strip is broken. Such a strip is called an open strip. Furthermore, the location of the rupture, e.g. on the silicon strip, in the Kapton cable or on a bond wire, makes a difference on the value of the noise.

In cases where the bond wire connecting the Beetle with the pitch adapter (PA) on a M hybrid is broken, the ENC of the channel will decrease by about 1840. This huge difference in noise is illustrated in Figures 3.1(a) and 3.1(b), where raw noise measurements for a redout channel having a broken bond at the PA recorded in 2006 and 2009 respectively are shown. Due to the clear difference in raw noise, broken bonds (at the PA) are likely to be detected by applying a single cut on the raw noise. This will be described in more detail in Section 3.1.

3.1 Hard Cut

Due to the clear signature in raw noise of open channels and the steep edge at the left-hand side of the noise distribution (see Figure 2.9) a single cut can be used to define low noise channels. The cut is applied over all the TT detector and is referred to as the hard cut. As the left-hand side edge of the noise distribution is dominated by the noise distribution for L type readout sectors (see Figure 2.10), a possible definition using the modified noise calculation as described in Section 2.5 for the hard cut is based on the mean and the rms of the latter. The mean and the rms of the noise distribution for L type readout sectors were determined for different runs,

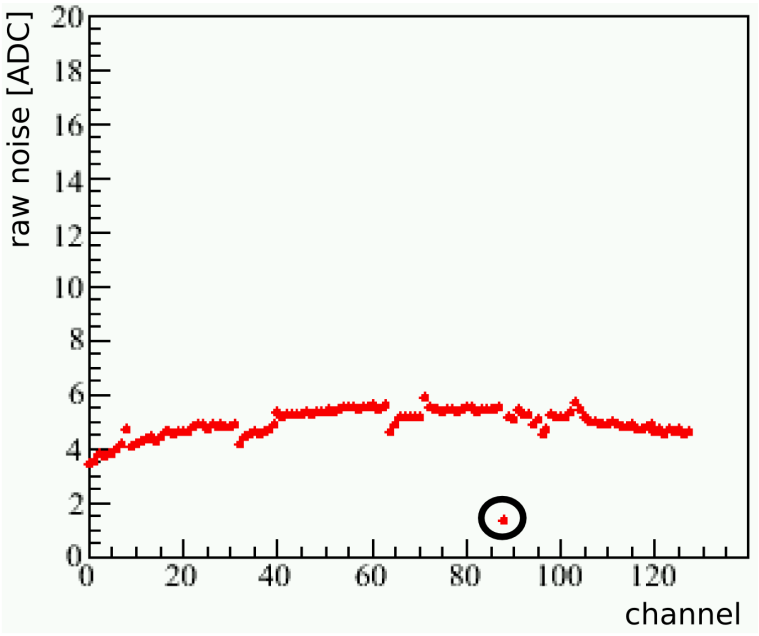

(a)

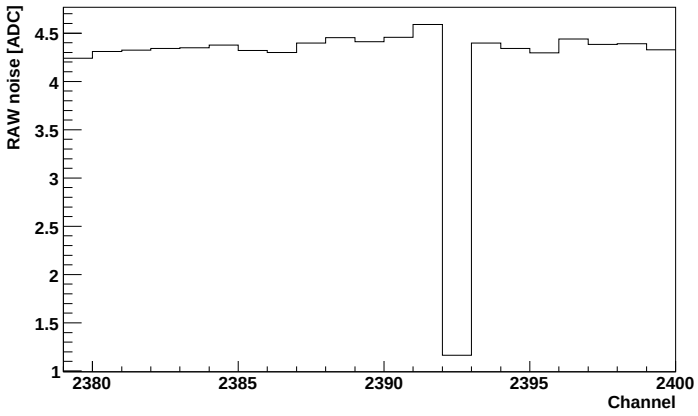

(b)

Figure 3.1: Raw noise measurement for channel 2392 TELL1 board No. 18:
(a) Raw noise measured in the Zurich laboratory in May 2006 as a function of the channel number of the Beetle. For module quality tests, different labels were used. The circle marks the noise measurement of channel No. 88 of Beetle No. 2 on the M sector of the half-module TT45, which corresponds to channel 2392 of TELL1 board No. 18 Due to a broken bond at the pitch adapter this channel shows low raw noise of 1.25 ADC already in early quality assurance tests. A Noise measurement for this channel made with the fully operational TT detector in 2009 is shown in Figure (b).
(b) Raw noise as a function of the channel number (2380–2400), measured in 2009 of the TELL1 board No. 18. Channel 2392 shows low noise of 1.15 ADC caused by a broken bond on the PA. A Noise measurement for this channel made during quality assurance tests in 2006 is shown in Figure (a).

see Table 3.1. As

$$\mathrm{avg}_{\mathrm{mean}} - 5 \times \mathrm{avg}_{\mathrm{rms}} \simeq 1.764\,\mathrm{ADC},$$

a (conservative) hard cut of 1.75 ADC was obtained. This cut might be subject to tuning in the future. Figure 3.2 illustrates the effect of the hard cut. The noise distribution for all channels is drawn in black. In red, the noise distribution of channels having noise smaller than 1.75 ADC is shown.

LHCb run No.	mean [ADC]	rms [ADC]
48435	2.479	0.147
46819	2.478	0.147
46054	2.476	0.145
44288	2.485	0.146
43225	2.477	0.144
35605	2.513	0.155
average	2.501	0.147
stdDev	0.044	0.004

Table 3.1: This table contains the mean and rms values of noise distributions for L sectors for different runs. Any channel having a known problem was rejected to determine these values.

Due to broken bonds in between two sensors within a sector, any disconnection on the silicon strip or the Kapton cables, the total capacitance of the strip decreases. However, the decrease is expected to be smaller compared to when the connection is broken at the pitch adapter. Therefore a slightly decreased raw noise is expected. Due to the faint signature in raw noise, this kind of open channels might fail the hard cut.

3.2 Soft Cut

To find channels having a lower noise than general noise level in a port, but failing the global hard cut, a cut criterion considering local properties of the noise, i.e. the noise level on the port, was investigated. A channel failing the hard cut but fulfilling the soft cut will be called a soft low noise channel. In order to determine the noise level in a port, a straight line was fitted to the noise (Figure 3.3). The resulting line was used to calculate the expected noise n_{fit} for each channel. For a given channel, the difference between the measured noise n and the expected noise n_{fit} is used to apply the so-called soft cut:

$$\Delta n = n - n_{\mathrm{fit}} < \text{soft cut}.$$

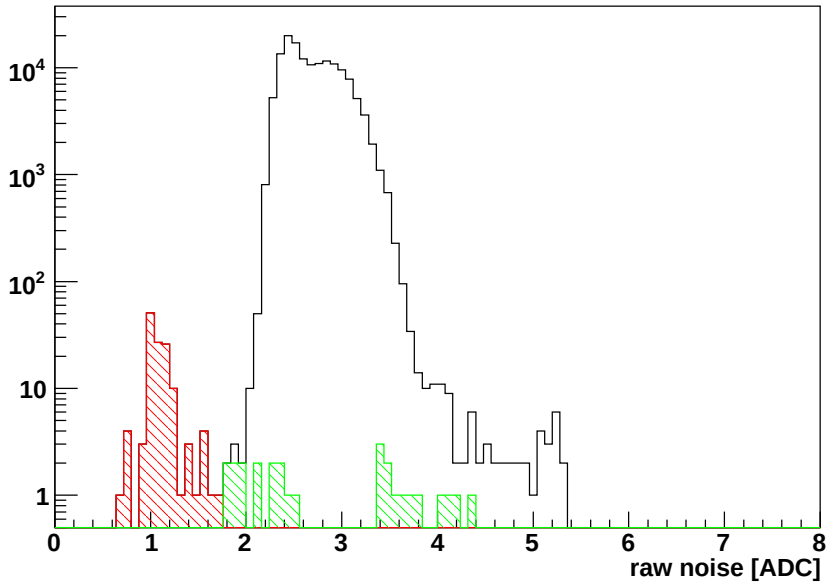

Figure 3.2: The raw noise distribution for all strips is drawn in black. The noise distribution of channels selected with a hard cut of 1.75 ADC is drawn in red. In green: the distribution of the noise of soft low noise channels selected with a soft cut of −0.5 ADC (see Section 3.2). Data is from run 50076.

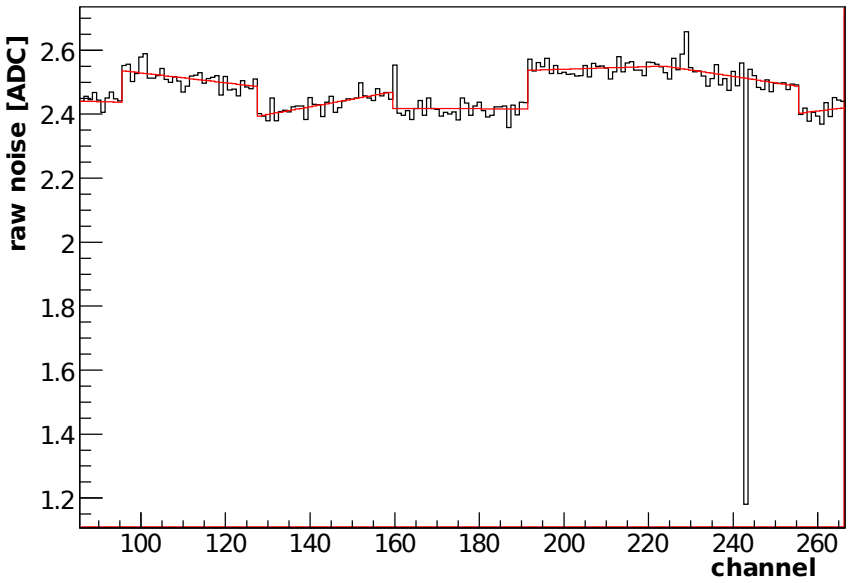

Figure 3.3: The raw noise on a few channels is drawn in black. In red the line fitted to the noise level on the port is fitted.

The distribution of the difference Δn for all channels of the detector is shown in Figure 3.4. There are two peaks: a main peak at 0.1 ADC and a small one at -1.6 ADC. For low noise channels ($n <$ hard cut), the distribution of Δn peaks at -1.6 ADC and is drawn in red. The distribution of the noise of soft low noise channels is drawn in green colour in Figure 3.2.

Based on data from eight different runs (run 0 – 7, see Table 2.1.) an estimation for the soft cut was obtained as follows. For a given soft cut, the number of soft low noise channels of the TT detector was determined (No. of selected channels). Assuming that a channel is affected by a problem causing lower noise, one expects that it will fulfill these requirements regularly in all measurements. A channel fulfilling the soft cut in every of the eight runs is considered as stable (No. of stable channels). Figure 3.5 shows the number of selected channels (black) and the ratio of stable and selected channels (red) as a function of the soft cut. As expected, the number of selected channels increases when weaker soft cuts are applied. A purity of the selected sample is estimated to be 85 % obtained with a soft cut of -0.5 ADC and using the modified noise calculation described in Section 2.5.

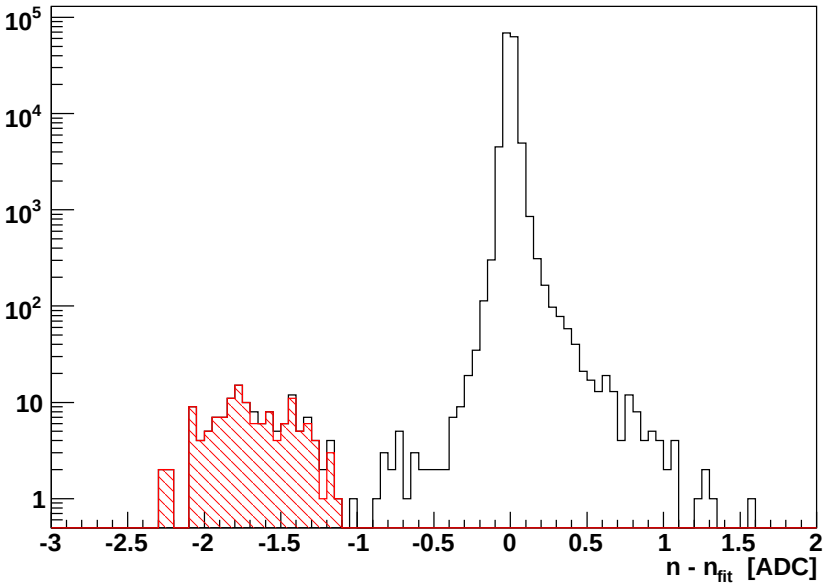

Figure 3.4: This is the distribution of the criterion for the soft cut, i.e.$\Delta n = n - n_{fit}$. The distribution of Δn for low noise channels failing the hard cut $of n <$1.75 ADC is drawn in red. Data is from run 50076.

To get an idea of the behaviour of unstable soft low noise channels, Δn was plotted as a function of the run number in Figure 3.6 for five unstable channels determined with a soft cut of -0.4 ADC (see Table A.3). Most

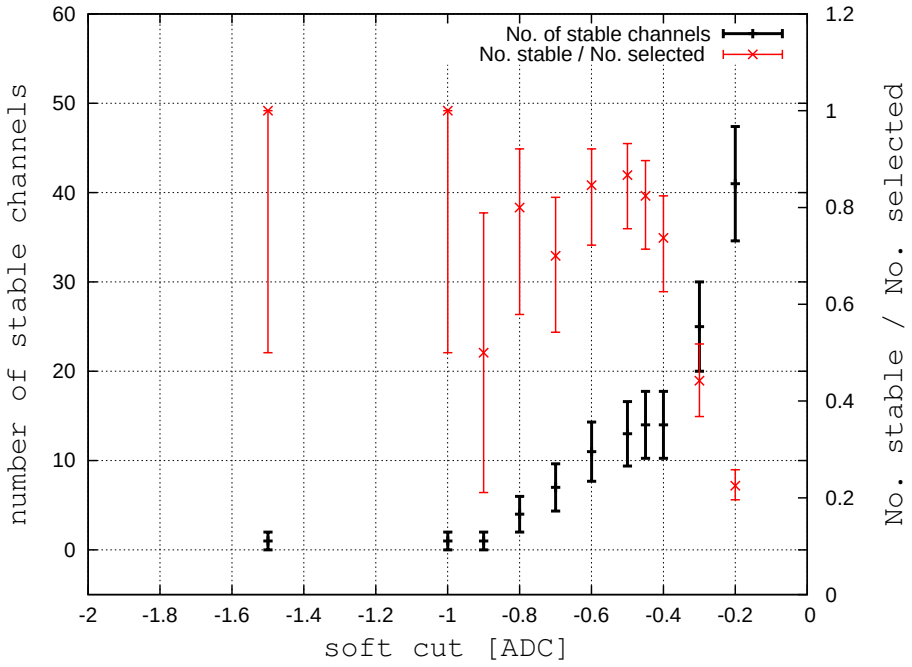

Figure 3.5: The number of stable channels and the ratio of stable versus selected channels (i.e. the purity) is plotted versus the soft cut value. The modified noise calculation as described in Section 2.5 was used. The data of 8 runs, i.e. run 0 – 7 (see Table 2.1) was taken into account. Plot based on numbers indicated in Table A.2.

interesting is channel 1976 on TELL1 No. 6, as this one is located within a region affected by the broken bond problem (see Section 3.3) and seems to fulfilling the soft cut in run 1.

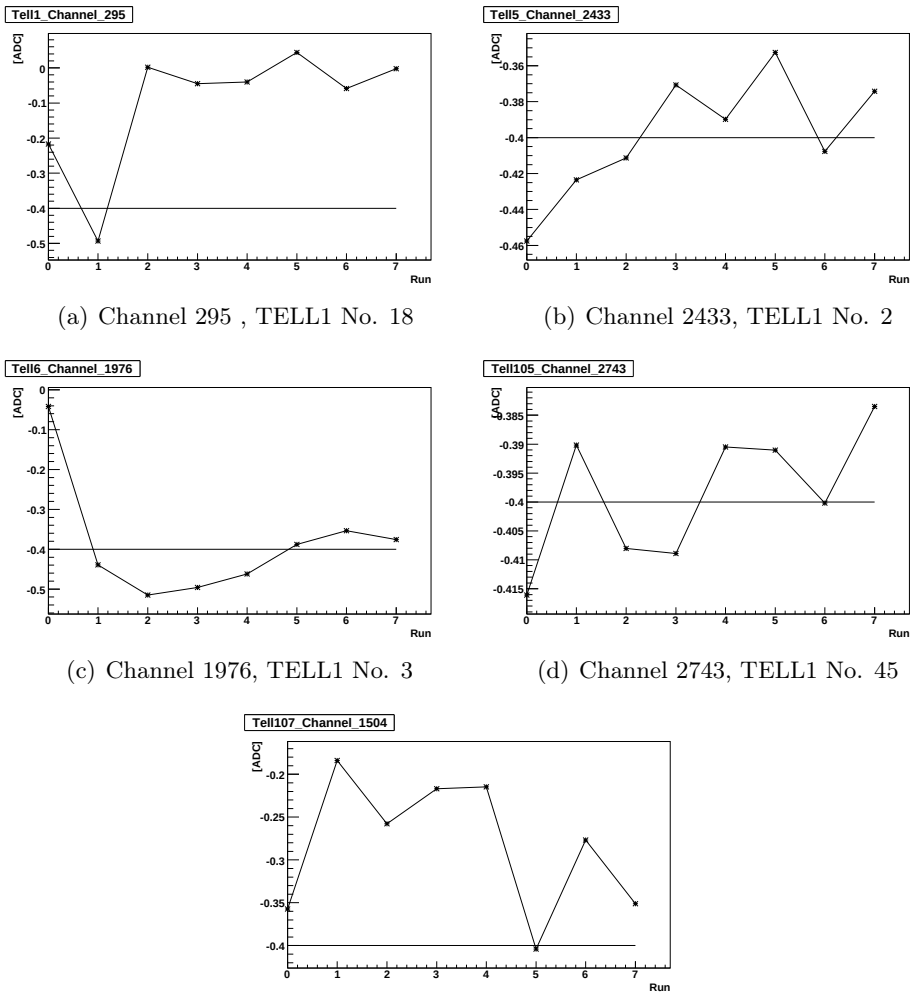

(a) Channel 295 , TELL1 No. 18

(b) Channel 2433, TELL1 No. 2

(c) Channel 1976, TELL1 No. 3

(d) Channel 2743, TELL1 No. 45

(e) Channel 1504, TELL1 No. 47

Figure 3.6: These plots show the difference Δn as a function of the run number. These channels fulfilled the soft cut of -0.4 ADC at least once, but were not considered as stable soft low noise channels. The run number on the x-axis of the plot corresponds to an LHCb run number, see Table 2.1. Please note the different scales.

3.3 Broken Bonds

After the installation of the TT detector it has been observed that the innermost row of bonds connecting the Beetle with the pitch adapter have started to break on 9 different readout sectors. Within a sector, the breaking start on one edge of the sensor and then evolves with time. This is referred to as the broken bond problem.

The four layers of bond wires connecting the channels of the Beetle to the pitch adapter can be seen in Figure 1.5. Figure 3.7 shows a closeup of the innermost row of bond pads (top) and the second row of bond pads (bottom). On the PA one can see that all bonds of the innermost row, except for the third from left, are broken at the heel of the bond foot. A detailed view of the third bond is provided in Figure 3.8. This bond seems to be close to breaking, a crack is visible at the heel of the bond. The reason for the breaking of these bonds is still under investigation.

Channels having broken bonds at the PA show a raw noise value of approximately 1.1 ADC. Figure 3.1(b) shows the effect on the noise pattern for the case of a single broken bond at the PA on channel 2392. In case every bond of the innermost row is broken, this leads to a noise pattern where every fourth channel shows low noise, e.g. see Figure 3.9. Near-to-breaking bonds might develop cracks at the ankle of the bond feet, as shown in Figure 3.8. Due to the partial connection a slightly lower noise could be expected and pinpoint to bonds in the process of breaking. These might be detected by the soft cut.

The tape used to patch the carrier of the Beetle chips and the PA onto the ground plate of the halfmodule is flexible and could allow a movement of these components and cause breaking of bonds. To investigate in situ whether an additional fixation of the pitch adaptor and the carrier of the Beetle chips with respect to the ground plate would prohibit further breaking of bonds, glue was put on the hybrid corresponding to TELL1 No. 3, sector 3, on 1 December 2008. For this readout sector, the noise pattern for subsequent runs within the period from 17 October 2008 until 30 June 2009 is given in Figure 3.9. One can observe the breaking of additional bonds in the noise pattern within this period.

As a slightly lower noise might point to breaking bonds, all channels of this sector were checked with a loose soft cut of -0.3 ADC on data from eight runs[1]. Twenty channels fulfilled this soft cut at least in one run. Noise n and the difference Δn of these channels are plotted as a function of the run number in order to investigate the process of breaking. The plots are attached in Appendix A.2. Glue was put on the hybrid between run 0 and 1.

A rough characterisation of the observed process of breaking is given in

[1] Runs 0 – 7, see Table 2.1.

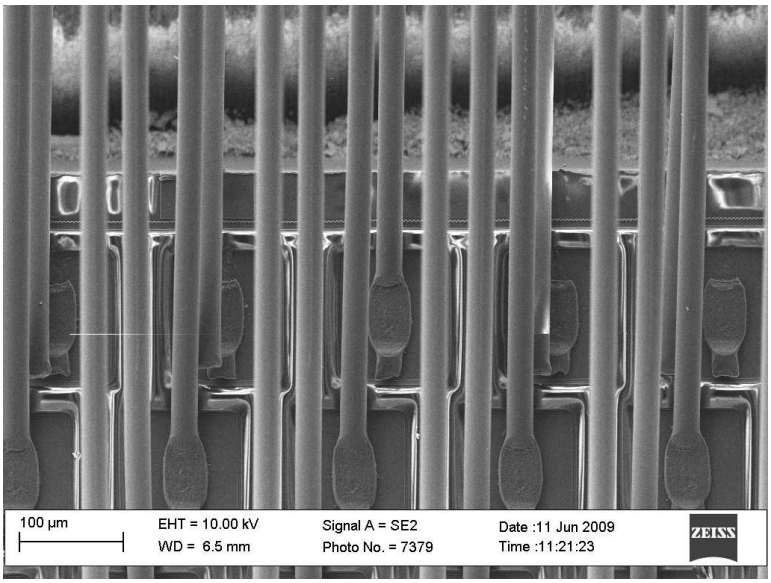

Figure 3.7: A picture of broken bonds taken with the electron-microscope [13]. All bonds in the innermost row are broken, except for the third bond (l.t.r) in the upper row. This is bond 11 on the M hybrid, Beetle 0, module TT175 and shown in detail in Figure 3.8. The bonds of the second row all do connect properly.

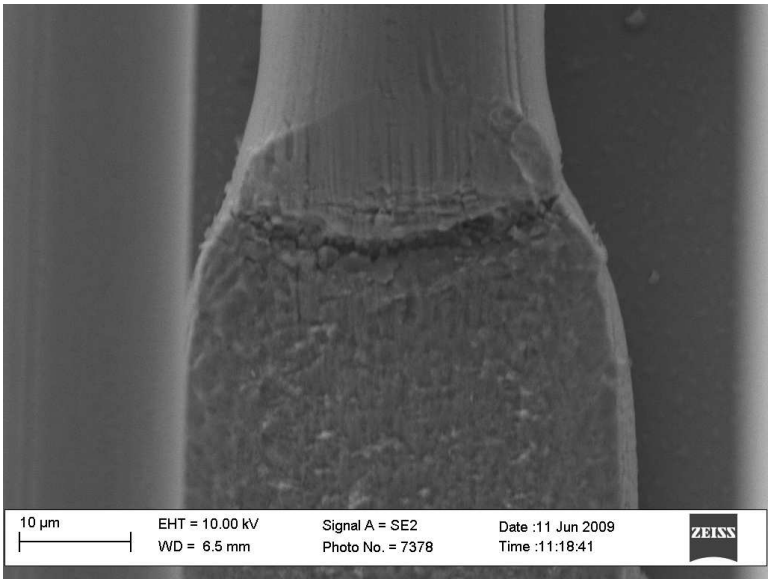

Figure 3.8: Not yet broken bond wire, as mentioned in Figure 3.7. A crack at the ankle of the bond foot can clearly be seen [13].

Table 3.2. Based on the data taken into account, a slow decrease in noise can be reported for one channel only, i.e 1928 on TELL1 No. 3, but even in this case, a transition through all three states - normal noise, soft low noise channel, low noise channel - was not detected. This channel might pinpoint a breaking in process as there it has a bond on the innermost row. However, the channel is not broken until 30 June 2009. The decrease in noise in between 31 March and 22 April for channel 2016 on TELL1 No. 3 to about 1.6 ADC fulfils the hard cut immediately and therefore is counted as an immediate broken channel. Most of the channels, i.e. 12, broke already before the first measurement was done and therefore have a rather stable noise of about 1.1 ADC. Five channels break without an observed announcement in the raw noise. Channel 1892 is recovering in run 4 and falling back to the low noise level again in the following run. Recovering might happen when a broken bond wire still might have loose contact, however this is is not understood.

noise is...	number of channels	channels
rising	1	1976
decreasing	5	1888, 1992, 2028, 1944, 2016
slowly decreasing	1	1928
~ 1.1 [ADC]	12	1880, 1884, 1896, 1900, 1904, 1912, 1924, 1932, 1956, 1960, 1972, 2040
recovering	1	1892

Table 3.2: This table gives a rough characterisation of the noise as a function of the run number for the channels of TELL1 No. 3 selected with a soft cut of -0.3 ADC and located on the glued hybrid. The plots are attached in the appendix, see Section A.2.

According to the analysis done, the observed breakings happened immediately and were not announced by a slight decrease in noise. Channel 1928 on TELL1 No. 3 however shows a slow decrease in noise over time and is due to its bond on the innermost row a candidate for breaking. In addition for channel 2016 on TELL1 No. 3 taking more data into account might unveil a slow breaking. Tuning the analysis therefore might lead to a better understanding of the process of breaking. In particular, taking into account more data in shorter time steps might enhance the sensitivity of the analysis.

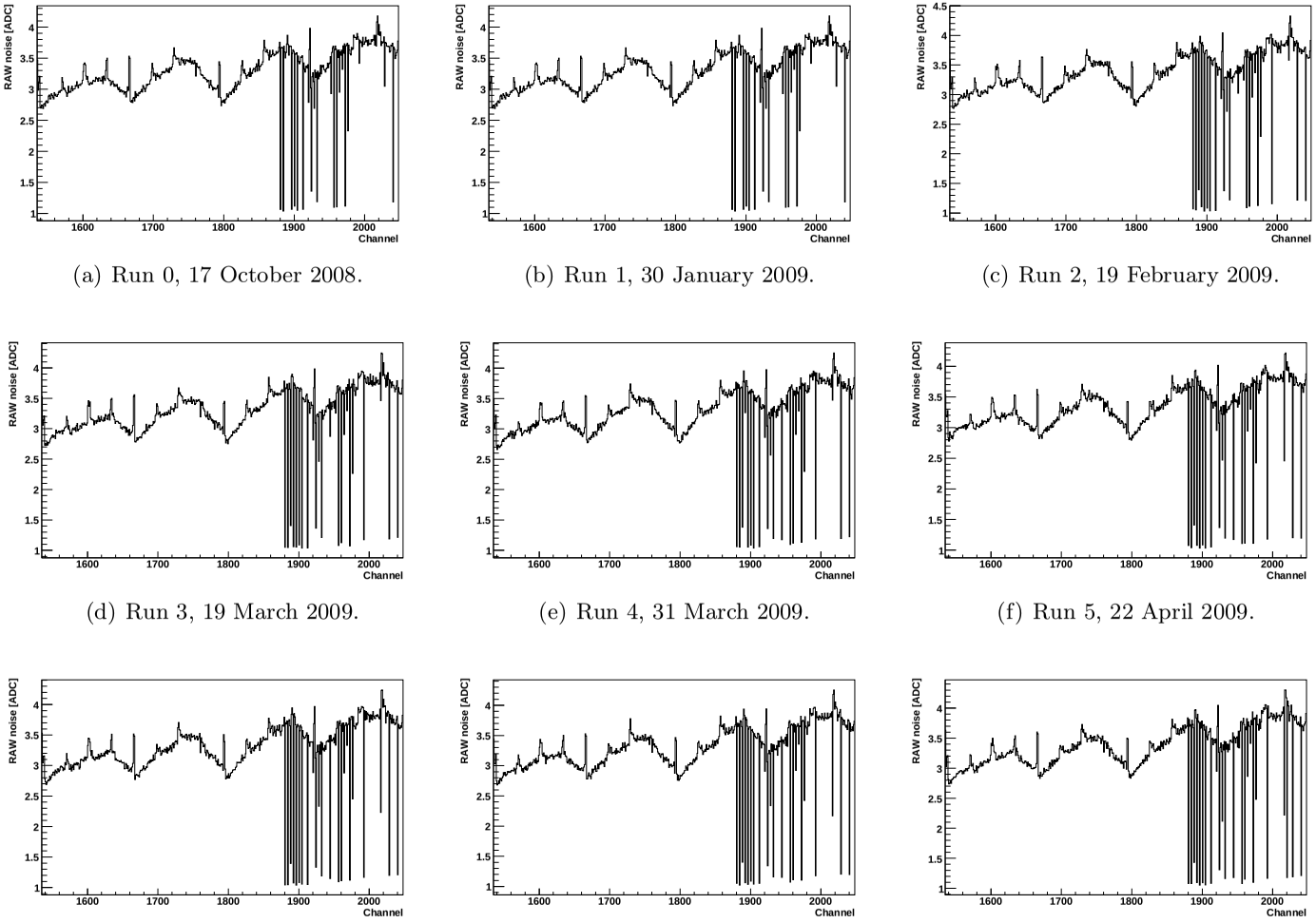

(a) Run 0, 17 October 2008.

(b) Run 1, 30 January 2009.

(c) Run 2, 19 February 2009.

(d) Run 3, 19 March 2009.

(e) Run 4, 31 March 2009.

(f) Run 5, 22 April 2009.

(g) Run 6, 3 June 2009.

(h) Run 7, 3 June 2009.

(i) Run 8, 30 June 2009.

Figure 3.9: Raw noise of TELL1 No. 3, sector 3, corresponding with the glued hybrid.

Chapter 4

Summary and Outlook

In the first part of this thesis, the noise calculation for the Tracker Turicensis of the LHCb eperiment was modified using header configurations and the effect of the pipeline column number (PCN) on pedestals. The spread of ADC values for a total of eight different configurations of the header and the parity of the PCN were determined and averaged. As a result, raw noise is reduced with respect to the default noise calculation. This new calculation removed the effect of the header cross talk on the raw noise. An effect related to the parity of the PCN on the pedestal height is reported; when the PCN is odd the pedestal is higher than when the PCN is even. The difference is up to 5 ADC counts, increasing towards the middle channels of the Beetle and as a function of the channel number of the readout sector. The effect is smaller for long readout sectors which have silicon micro strips of about 40 cm length. Whether it will be desired, and to which extent it will be possible, to implement the method in the ST software is under discussion.

In the second part, low noise channel monitoring based on raw noise data is described. Two cut criteria are introduced:

- A hard cut is applied on the raw noise. It is sensitive to stable low noise channels and was set to 1.75 ADC. This cut defines low noise channels.
- A soft cut is applied to the difference between the measured raw noise and the expected noise according to the noise level of the neighbouring channels in the same port. The local noise level on the port is determined by fitting a straight line to the noise on the port as a function of the channel number. Channels failing the hard cut and fulfilling the soft cut are called soft low noise channels. A soft cut achieving a reasonable purity is estimated as -0.5 ADC. However, further tuning with more statistics and error calculation is needed.

The process of breaking of bond wires was investigated using the soft cut. In particular it was studied whether it was possible to pinpoint to

channels in the process of breaking by assuming that the breaking of bonds is announced by a slow decrease of the noise. Slow decrease in noise over a long term is observed in one channel only. Tuning the analysis might lead to a better understanding of the process of breaking. In particular, taking into account more data in shorter time steps might enhance the sensitivity of the analysis.

Acknowledgments

Accomplishing this work was only possible with the support of the LHCb research group at the University of Zurich. First of all I would like to thank Prof. Ulrich Straumann who gave me the chance to work on this very exciting project and always offered encouraging advice during my studies. Next I would like to thank my supervisors Dr. Olaf Steinkamp and Dr. Jeroen van Tilburg for sharing their knowledge, providing help whenever needed and the correction of my thesis.

Many thanks also go to all colleagues of the LHCb and CTA research groups here in Zurich for the pleasant working atmosphere, all the fun during office and evenings hours and their helpful assistance. A special thanks goes to Dr. Mark Tobin for the corrections of my thesis.
Thanks everyone who supported me in word and deed.

Bibliography

[1] P. Lefèvre and T. Petterson, The Large Hadron Collider: conceptual design, CERN-AC-95-05-LHC (1995)

[2] Phillip Sievers. A Silicon Inner Tracker for the LHCb Experiment. PhD thesis, University of Zurich (2002).

[3] S. Löchner, M. Schmelling, The Beetle Reference Manual, LHCb internal note, 2005-105 (2005).

[4] F. Legger, A. Bay, G. Haefeli, L. Locatelli, TELL1, a common readout board for LHCb, LHCb internal note, LHCb-2004-100 (2004).

[5] S. Koestner, U. Straumann, Noise Considerations of the Beetle amplifier used with long silicon strip detectors, LHCb internal note, 2005-029 (2005).

[6] LHCb Technical Design Report Reoptimized Detector Design and Performance, CERN-LHCC-2003-030 (2003).

[7] A. Papadelis, VELO sensor Signal-to-Noise performance in ACDC3, LHCb internal note, 2009-003 (2009).

[8] L. Locatelli, Tests on the VeLo analogue transmission line with the TELL1 prototype RB3, LHCb internal note 2004-086 (2004).

[9] U. Bieler, Contributions to noise in the data readout for Trigger Tracker in the LHCb Experiment, Master Thesis, ETH Zurich (2007).

[10] M. Agari et al., Test-Beam Measurements on Prototype Ladders for the LHCb TT Station and Inner Tracker, LHCb internal note 2003-082 (2003).

[11] J. Gassner, M. Needham, O. Steinkamp, Layout and Expected Performance of the LHCb TT Station, LHCb internal note, 2003-140 (2004).

[12] G. Landolt, Setting up an LHCb TT-Detector Test Stand, Bachelor Thesis, University of Zurich (2009).

[13] S. Steiner and K. Escher, University of Zurich, private communication (2009).

Appendix A

Appendix

A.1 Varia

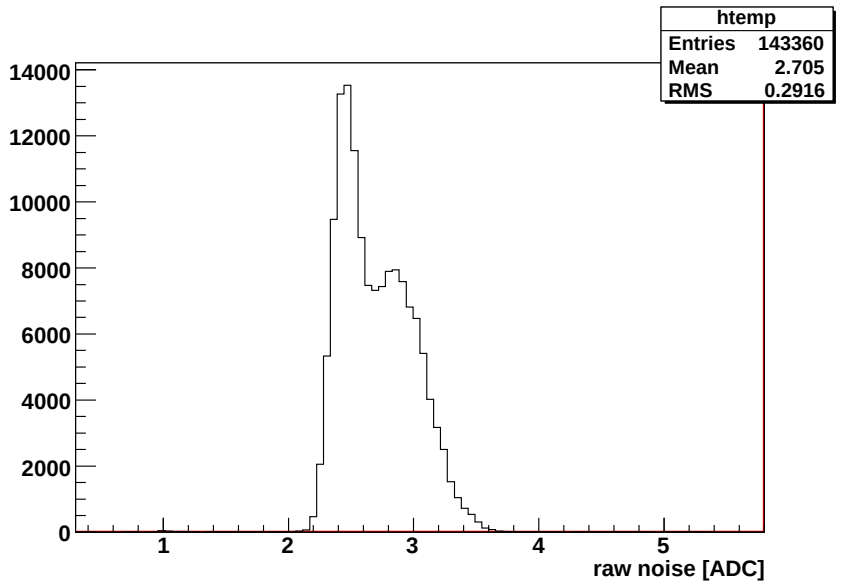

Figure A.1: Noise distribution for all strips of the TT detector of data recorded in run 52076. Noise calculated with the modified method.

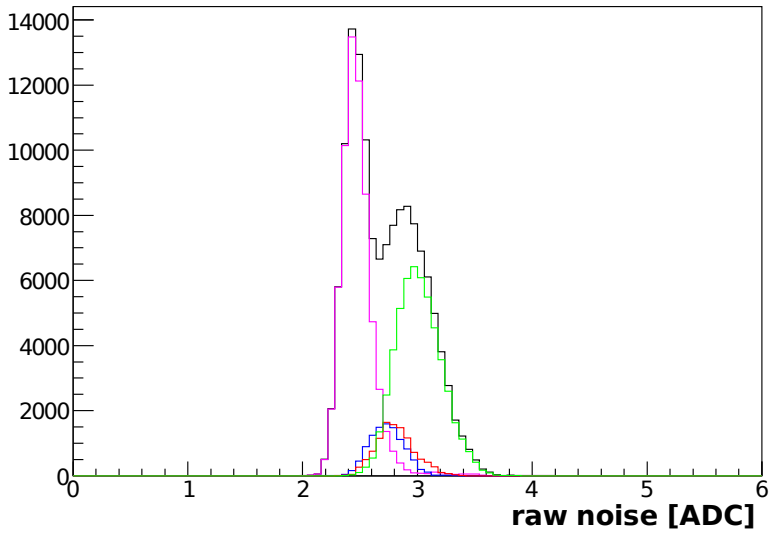

Figure A.2: Noise distributions for readout sector types. Noise distribution of all TT sectors (black), strips of L type sectors (pink), strips of M2 type sectors (red), strips of M3 type sectors (green), strips of K type sectors (blue). Noise calculated with the modified method. Low noise channels, i.e. $n < 1.75$ADC, channels having any other strip status than OK and the first and the last of the readout sector were rejected to draw the distributions. Data is from run 51737.

Tell No.	Channels	Total	Sector Type
7	2049, 2560	2	L
21	2049,2560,2561,3072	4	L
25	3072	1	L
28	2561,2562	2	L
43	1554 – 1557	4	M3
43	2025 – 2033	13	M3
44	1547 – 1566,	20	L
44	2020 – 2038,	19	L
		65	

Table A.1: The table lists high readout channels having noise n >4 ADC in run 52076. See Figure 2.9.

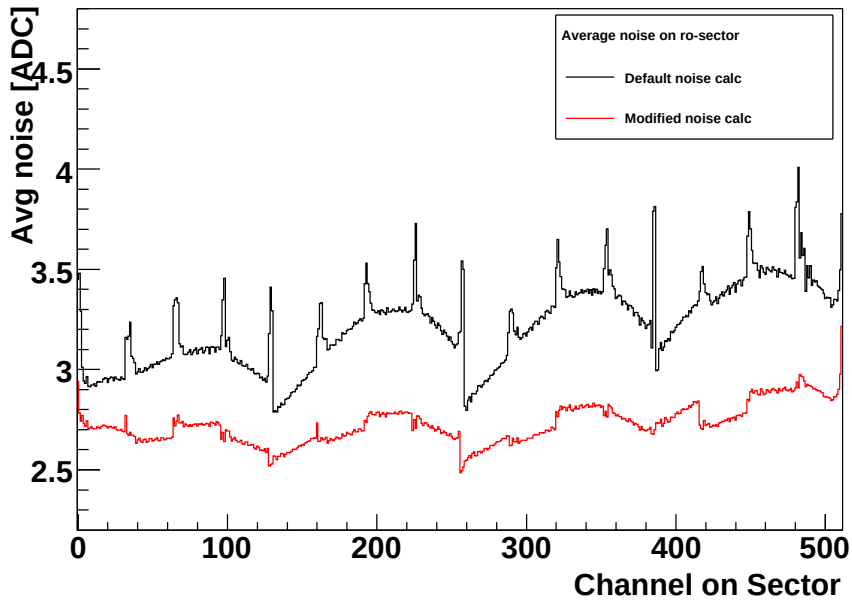

Figure A.3: The plot shows the noise versus channel number (0–511) averaged over all readout sectors. Two different methods to calculated the noise are compared. Assuming a fully enabled readout chain, there are 280 readout sectors.

			purity	
soft cut [ADC]	selected	stable	lower limit	upper limit
-0.2	182	41	0.196	0.258
-0.3	43	19	0.368	0.518
-0.4	19	14	0.626	0.824
-0.45	17	14	0.714	0.897
-0.5	15	13	0.756	0.932
-0.6	13	11	0.722	0.921
-0.7	10	7	0.542	0.821
-0.8	5	4	0.579	0.921
-0.9	2	1	0.211	0.789
-1.0	1	1	0.500	1.000
-1.5	1	1	0.500	1.000

Table A.2: The estimation of the soft cut is based on the numbers indicated here. *Selected:* Number of channels selected by applying a given soft cut. *Stable:* The number of stable channels indicates how many of the channels fulfilled the requirements in each of the 8 runs taken into account, i.e. run 0 – 7, see Table 2.1. *Purity:* The purity of the selected sample, i.e. the ratio $\frac{\text{stable}}{\text{selected}}$. *Lower (upper) limit:* The limits indicate the 68% confidence interval of the purity.

TELL1	channel	cut fulfilled in # runs
1	295	1
5	2433	4
6	1976	4
105	2743	4
107	1504	6

Table A.3: Applying a soft cut of -0.4 ADC, i.e diff < -0.4ADC, 19 channels fulfilled the cut at least once, as indicated in table A.2. 14 channels fulfilled the cut criteria in all eight runs and are considered as stable with respect to the soft cut. The five channels listed in this table did not fulfil the cut criteria in every run. Eight runs were taken into account, i.e. run 0 – 7, see table 2.1.

A.2 History plots for the glued Hybrid, TELL No. 3

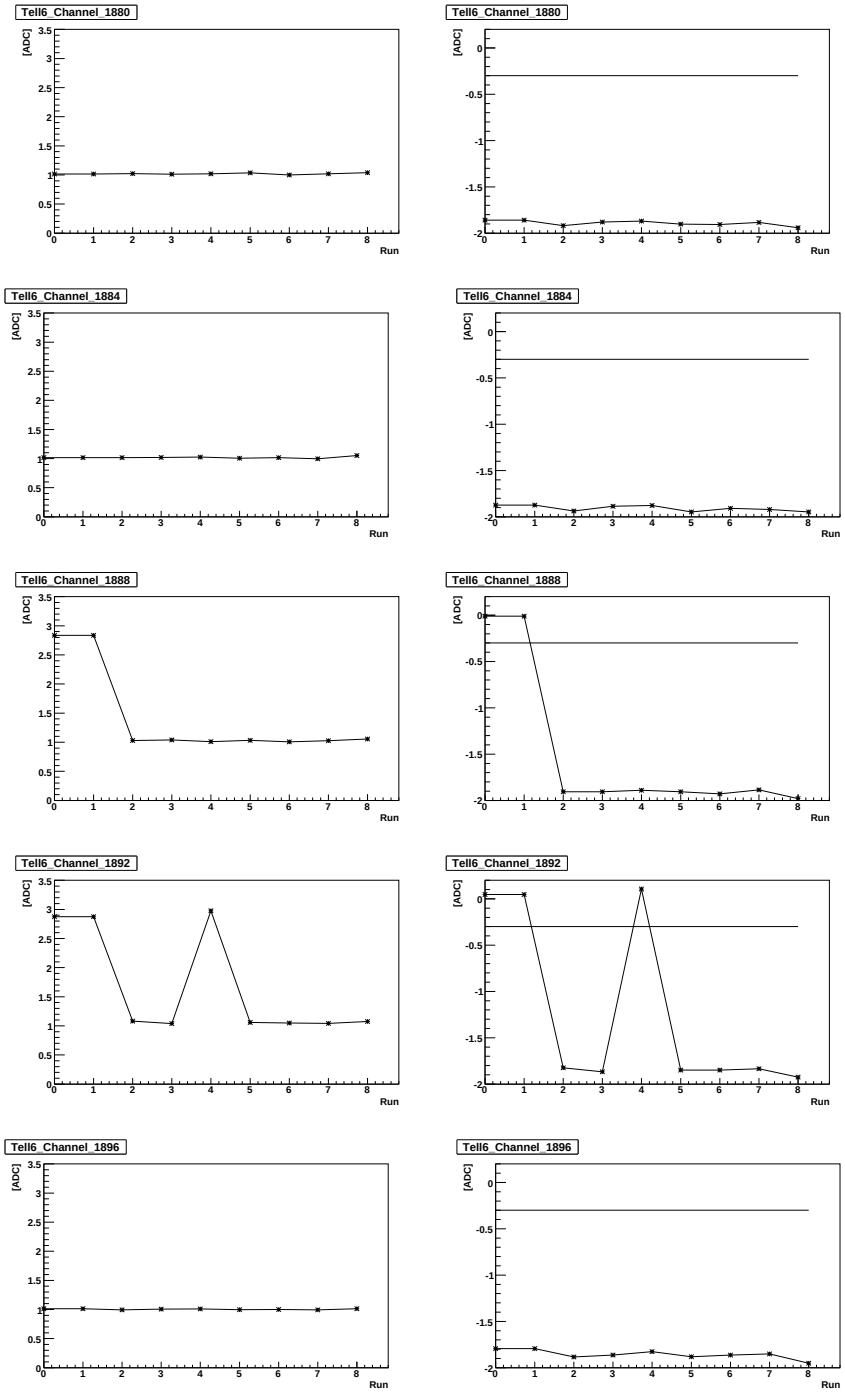

Figure A.4: History plots for the channels 1880 – 1896 of TELL1 No. 3 (corresponding TELL1 source-ID is 6), selected with a soft cut of -0.3 ADC. The plots on the left-hand side show the noise as a function of the run number. The plots on the right-hand side show the difference Δ_n as a function of the run number. The run number on the x-axis of the plot corresponds to an LHCb run number, see Table 2.1.

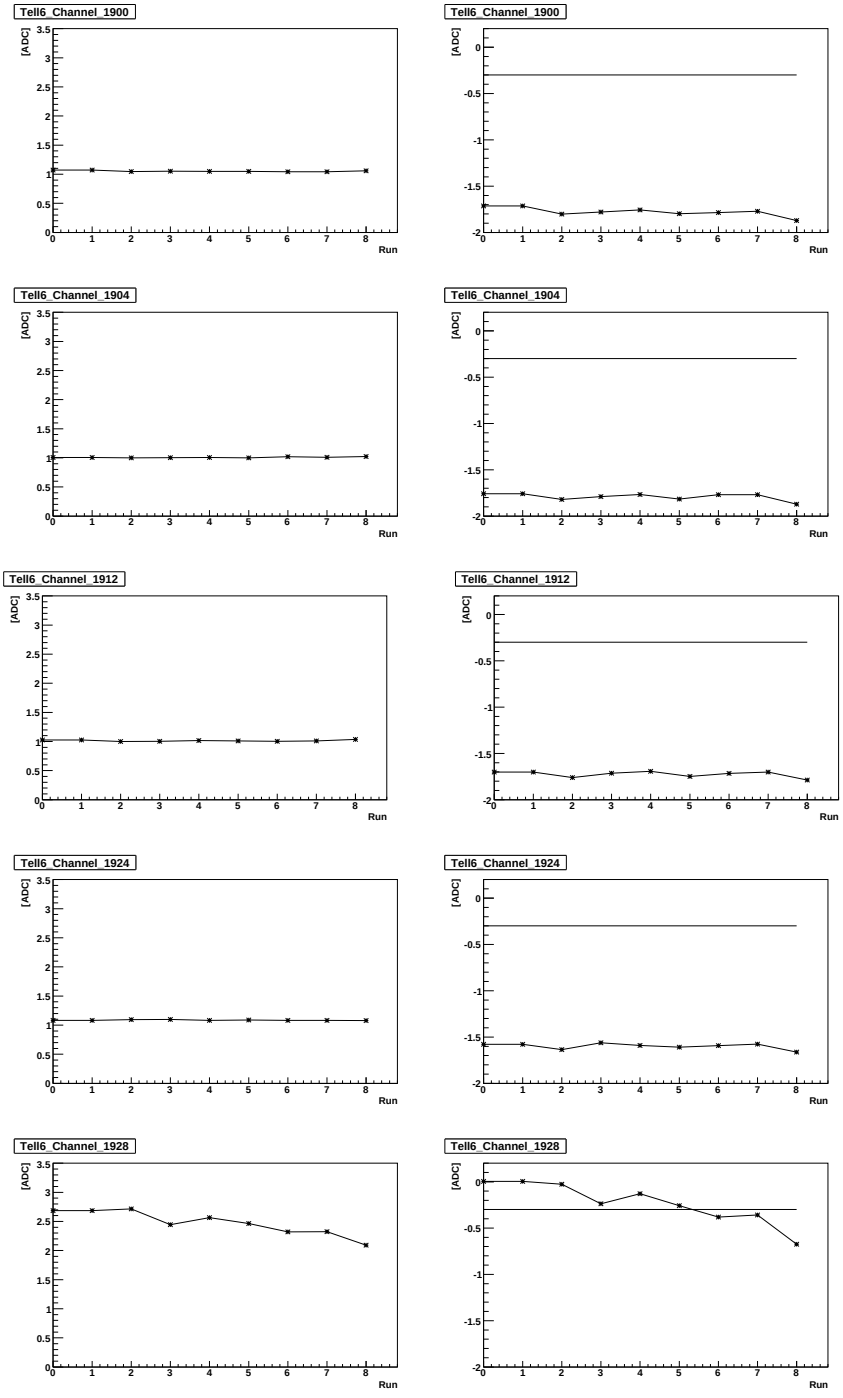

Figure A.5: History plots for the channels 1900 – 1928 of TELL1 No. 3 (corresponding TELL1 source-ID is 6), selected with a soft cut of -0.3 ADC. The plots on the left-hand side show the noise as a function of the run number. The plots on the right-hand side show the difference Δ_n as a function of the run number. The run number on the x-axis of the plot corresponds to an LHCb run number, see Table 2.1.

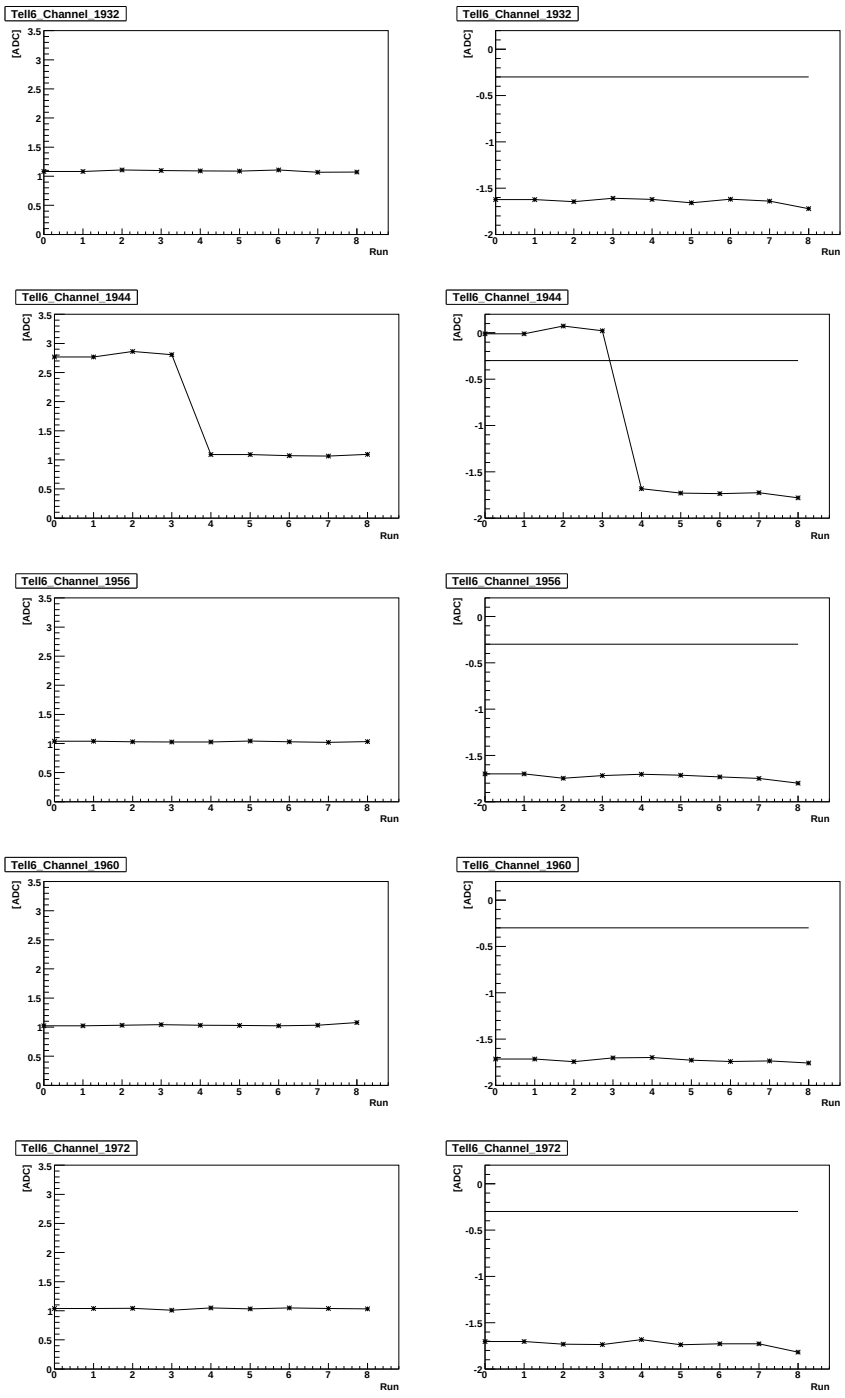

Figure A.6: History plots for the channels 1932 – 1972 of TELL1 No. 3 (corresponding TELL1 source-ID is 6), selected with a soft cut of $-0.3\,\mathrm{ADC}$. The plots on the left-hand side show the noise as a function of the run number. The plots on the right-hand side show the difference Δ_n as a function of the run number. The run number on the x-axis of the plot corresponds to an LHCb run number, see Table 2.1.

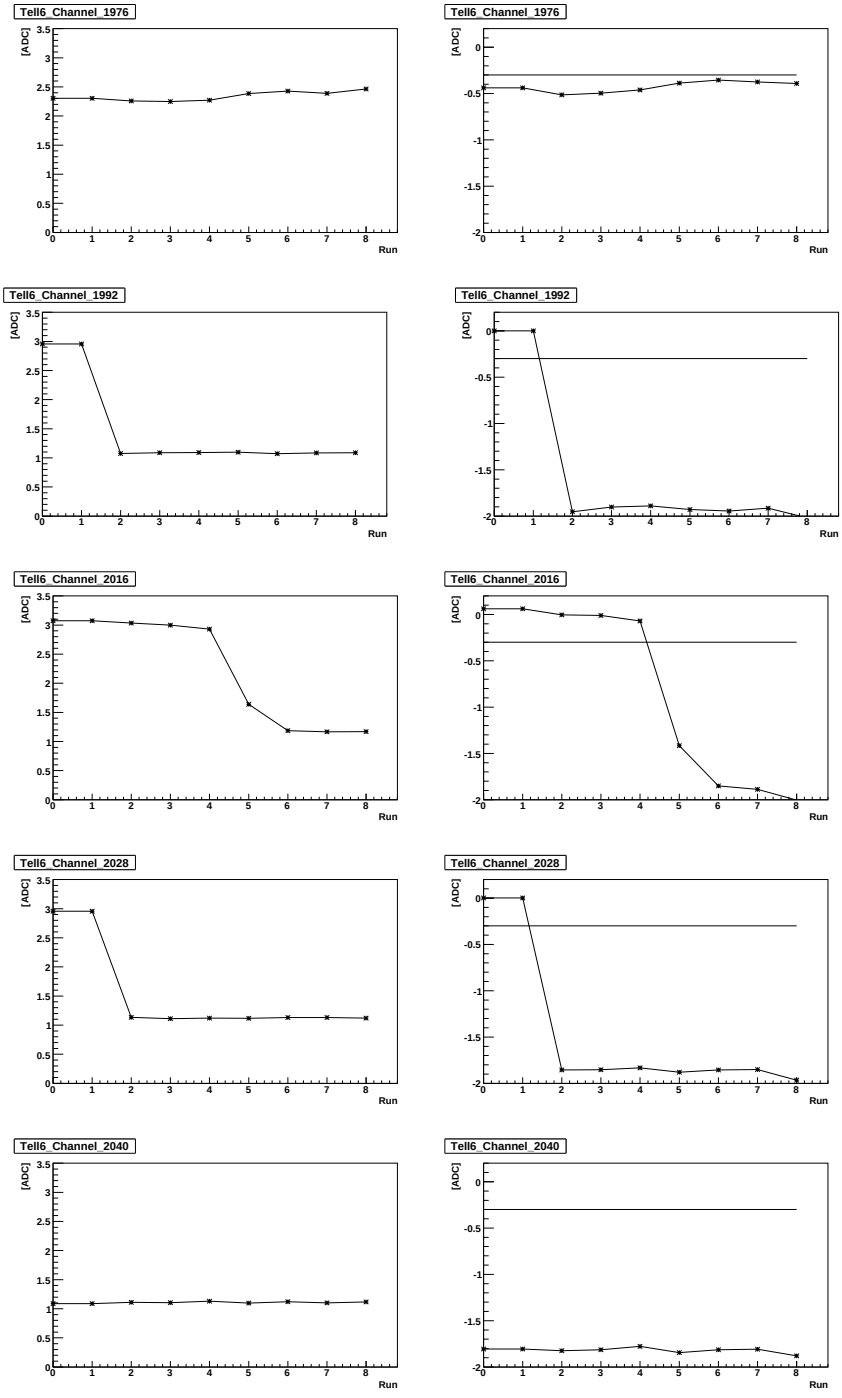

Figure A.7: History plots for the channels 1976 – 2040 of TELL1 No. 3 (corresponding TELL1 source-ID is 6), selected with a soft cut of -0.3 ADC. The plots on the left-hand side show the noise as a function of the run number. The plots on the right-hand side show the difference Δ_n as a function of the run number. The run number on the x-axis of the plot corresponds to an LHCb run number, see Table 2.1.